



1 On the dynamics of ozone depletion events at Villum 2 Research Station in the High Arctic

3 Jakob Boyd Pernov^{1,2}, Jens Liengard Hjorth¹, Lise Lotte Sørensen¹, and Henrik Skov¹

4 ¹Department of Environmental Science, iClimate, Arctic Research Center, Aarhus University, Roskilde, Denmark.

5 ²Extreme Environments Research Laboratory, École Polytechnique Fédérale de Lausanne, 1951 Sion, Switzerland.

6

7 *Correspondence to:* Jakob Boyd Pernov (jakob.pernov@epfl.ch) and Henrik Skov (hsk@envs.au.dk)

8 Abstract

9 Ozone depletion events (ODEs) occur every spring in the Arctic and have implications for the atmospheric
10 oxidizing capacity, radiative balance, and mercury oxidation. Here we comprehensively analyze ozone,
11 ODEs, and their connection to meteorological and air mass history variables through statistical analyses,
12 back-trajectories, and machine learning (ML) from observations at Villum Research Station, Station Nord,
13 Greenland.

14 We show that the ODE frequency and duration peak in May followed by April and March, which is likely
15 related to air masses spending more time over sea ice and increases in radiation from March to May. Back-
16 trajectories indicate that, as spring progresses, ODE air masses spend more time within the mixed layer and
17 the geographic origins move closer to Villum. ODE frequency and duration are increasing during May (low
18 confidence) and April (high confidence), respectively. Our analysis revealed that ODEs are favorable under
19 sunny, calm conditions with air masses arriving from northerly wind directions with sea ice contact.

20 The ML model was able to reproduce the ODE occurrence and illuminated that radiation, time over sea ice,
21 and temperature were the most important variables for modeling ODEs during March, April, and May,
22 respectively. Several variables displayed threshold ranges for contributing to the positive prediction of
23 ODEs vs Non-ODEs, notably temperature, radiation, wind direction, time spent over sea ice, and snow.
24 Our ML methodology provides a framework for investigating and comparing the environmental drivers of
25 ODEs between different Arctic sites and can be applied to other atmospheric phenomena (e.g., atmospheric
26 mercury depletion events).

27

28



29 1. Introduction

30 Globally, ozone is an important constituent of the stratosphere but it also plays a central role in the
31 tropospheric chemistry. Due to ozone's radiative properties, such as absorption in both the ultraviolet (UV)
32 and infrared (IR) regions, it serves as an important short-lived climate forcer (SLCF). The absorption of
33 UV light by ozone also leads to the formation of an O^{1D} atom, which reacts with water vapor to form
34 hydroxyl (OH) radicals, the most crucial oxidant in the troposphere. Tropospheric ozone sources include in
35 situ photochemical formation from the catalytic reactions involving nitrogen oxides (NO_x) and volatile
36 organic compounds (VOCs), which are initiated by OH but dependent on the ratio between NO_x and VOCs
37 (Seinfeld and Pandis, 2016). Stratosphere-troposphere exchange (STE) represents another significant ozone
38 source (Monks et al., 2015). Sinks of ozone include dry deposition and reactions with NO_x, hydrocarbons,
39 and halogens as well as photolysis driven loss.

40 During winter and spring in the Arctic, long range transport from the mid-latitudes and STE are the
41 major sources of ozone (Helmig et al., 2007a; Hirdman et al., 2010; Stohl, 2006). In the summertime Arctic,
42 low absolute humidity suppresses the formation of OH radicals and coupled with low primary emissions of
43 precursor species (VOCs and NO_x), in situ formation of ozone is limited (Ianniello et al., 2021; Morin et
44 al., 2008; Pernov et al., 2021). Dry deposition, photolysis, and reactions with halogens are the dominant
45 sinks while wet deposition is of less importance in the Arctic because of the low humidity and the limited
46 removal efficiency of ozone by precipitating snow/ice (Barten et al., 2021).

47 A phenomenon of the springtime Arctic, known as ozone depletion episodes (ODEs), involves the
48 rapid depletion of ozone due to catalytic reaction with halogen species (X or Y, representing Br, Cl, or I)
49 (Barrie et al., 1988; Simpson et al., 2007b, 2015; Skov et al., 2004). As shown in reactions (R) 1-6:

50



54

55 While ozone is catalytically destroyed by reactions R1 to R3, the number of available halogen
56 atoms is not increased. Multiphase reactions like the halogen explosion sequence (R1, R2, R4, R5, and R6)
57 accelerate halogen production, leading to high concentrations of ultra-reactive halogen species and causing
58 observed ODEs.



62

63 Moreover, ODEs occur simultaneously with atmospheric mercury depletion episodes (AMDEs)
64 (Schroeder et al., 1998), and the relative rate principle suggests that ODEs and AMDEs can be explained
65 by competing reactions of ozone and elemental mercury with Br atoms (Skov et al., 2004, 2020), which has
66 recently been demonstrated by direct measurements (Wang et al., 2019). The relative importance of ozone
67 removal by reactions with respectively Br and I atoms in spring is unclear (AMAP, 2015; Benavent et al.,
68 2022; Wang et al., 2019; Whaley et al., 2023). Recently, it was found that Br is the dominant oxidant during
69 spring, whereas I chemistry was active during the entire sunlight period (March to October) (Benavent et
70 al., 2022).



71 The sources for atmospheric halogens include sea spray aerosols, brine migration through ice and
72 snowpack, blowing snow, and frost flowers (Simpson et al., 2007b, 2015) and the relative importance of
73 the halogen sources depends on the location and time. Sea-ice surfaces, aerosol, and frost flowers have
74 gained significant interest as halogen sources in earlier investigations. Later studies indicate that frost
75 flowers are of minor importance (Abbatt et al., 2012; Simpson et al., 2007a). Friess et al. showed, using
76 trajectory analysis, that areas of first-year sea ice are correlated with high BrO levels (Frieß et al., 2004), in
77 agreement with later satellite observations for the Arctic (Bougoudis et al., 2020). First-year sea ice is saltier
78 than multi-year ice and therefore expected to be a greater source of halogens to the atmosphere, however,
79 studies have shown that both first- and multi-year ice are sources of halogens and ODEs (Bognar et al.,
80 2020; Peterson et al., 2019). Recycling of halogens on frozen heterogeneous surfaces such as sea salt aerosols
81 and snowpack are also important sources of halogens (Peterson et al., 2017, 2018; Pratt et al., 2013; Raso
82 et al., 2017).

83 Meteorologically, ODEs have been usually associated with sunny conditions and cold temperatures
84 (Simpson et al., 2015). High and low wind speeds have also been connected to ODEs, where high wind
85 speeds generate blowing snow (which are a source of halogens) and low wind speeds are associated with a
86 stably stratified boundary layer, which confine reactants and oxidants in the lower most atmosphere (Jones
87 et al., 2009). Halogen explosion events and ODEs have also shown to be temperature dependent (Koo et
88 al., 2012; Tarasick and Bottenheim, 2002). This is likely connected to the need for a frozen heterogeneous
89 surface (sea ice, snowpack, blow snow, and aerosols) required for halogen propagation (Burd et al., 2017;
90 Jeong et al., 2022), although other studies have not found such evidence (Halfacre et al., 2014; Jacobi et
91 al., 2010).

92 Despite numerous studies and significant progress in understanding Arctic tropospheric ozone, the
93 dynamics of O₃ are still not yet fully understood (Simpson et al., 2015; Whaley et al., 2023) and significant
94 questions remain, including: What is the contribution of different halogen sources to ODEs such as sea ice
95 surfaces (multi- vs first-year ice), snowpack emissions, or recycling on aerosol particles? What are the
96 conducive meteorological conditions for ODEs? What is the contribution of halogen activation of aloft vs
97 in the boundary layer? What is the relative importance of Br and I atoms to ODEs during spring?

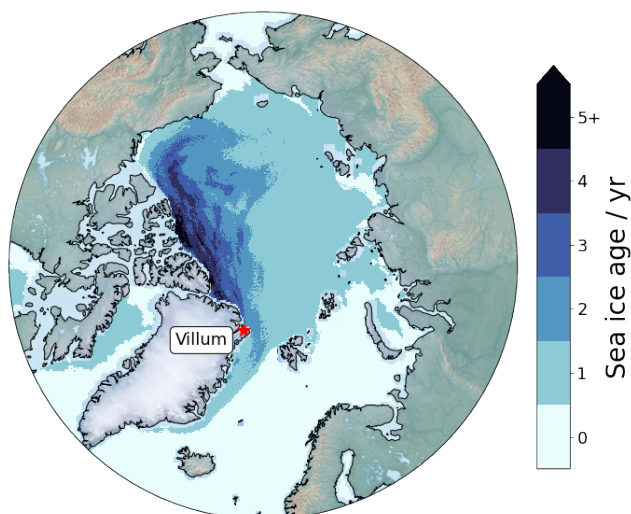
98 The lack of full understanding of halogen dynamics and the connection to ODEs makes it very
99 important to address the external variables that influence and determine the observed ozone concentrations
100 especially during ODEs. In the present paper, the connection to meteorological and air mass history
101 variables is studied to cast light on the variables that control ODEs. This is achieved through statistical
102 analyses, back-trajectories, and machine learning (ML) applied to ODEs observed at Villum Research
103 Station, Station Nord in Northeast Greenland from 1996 to 2019.

104 2. Methods & Materials

105 2.1. Site description

106 Villum Research Station (Villum) is located on a small peninsula in North East Greenland (Fig. 1). The
107 station is located at the Danish military outpost Station Nord (81° 36' N, 16° 40' W, 24 m a.s.l.). Ozone
108 measurements were conducted at Flyger's Hut from 1995 to 2014 and at the Air Observatory from 2014 to
109 present. They are located a few hundred meters apart and 2 km south of the central complex of Station Nord
110 and upwind of the station the majority of the time (> 95 %). No significant differences in ozone levels were
111 observed when moving measurement locations.

112



113

114 **Figure 1.** Location of Villum Research Station (Villum). Mean sea-ice age for March, April, and May
115 2007-2019, were taken from the National Sea & Ice Data Center (Tschudi et al., 2019)
116 (<https://nsidc.org/data/nsidc-0611/versions/4>). Map background made with data from Cross-Blend-Hypso
117 (naturalearthdata.com). The mean sea-ice age for individual spring months closely resembled the spring
118 mean, therefore the spring mean is displayed for clarity.

119 2.2. Atmospheric measurements

120 Sample air was drawn into a 20 cm i.d. electro-polished stainless-steel sampling line with a protective inlet
121 cap connected to a blower, where the ozone monitors sampled 0.8 L min^{-1} air. The setup is constructed to
122 avoid ice formation in the sample tube. Ozone is measured based on its absorption of UV light at 254 nm.
123 The original data was averaged to half hourly mean values and later reported to EBAS
124 (<https://ebas.nilu.no/>). Here we use 1-hour mean mixing ratios averaged from the native time resolution (15
125 min). The stability of the instruments is ensured by the addition of known concentrations of ozone from an
126 internal ozone generator traceable to a primary standard, in this way, although different instruments have
127 been employed, all use the same measurement and calibration methods, thus the measurements uncertainties
128 are estimated to remain unchanged. The Department of Environmental Science at Aarhus University is
129 accredited (EN 17025) to measure ozone but at Villum it is not possible to maintain the accreditation as the
130 visits to the station are not possible frequently enough. However, the instruments are operated as close as
131 possible to the accreditation procedures. To compensate for the deviations, two monitors are operated in
132 parallel. The uncertainty at a 95% confidence level is <7% for mixing ratios above 20 ppbv and 1.4 ppbv
133 for mixing ratios below 20 ppbv (Skov et al., 2004, 2020).

134 To quantify the frequency and the duration of ODEs, the parameter ‘ozone depletion hour’ was
135 defined as an hour during which the average ozone mixing ratio was below 10 ppbv, following the definition
136 used by other studies (Halfacre et al., 2014; Koo et al., 2012; Tarasick and Bottenheim, 2002; Yang et al.,
137 2020). In total, 6605 ODE hours were detected. To account for ozone mixing ratios exceeding 10 ppbv
138 during a single hour which was part of a larger depletion event, hours that were below 15 ppbv and the



139 previous and next hours were below 10 ppbv were also classified as ODEs. This resulted in 57 additional
140 hours being classified as ODEs, which brings the total number of ODEs to 6662, although this addition
141 criteria did not affect the results of this study.

142 **2.3. Meteorological variables**

143 Meteorological data were collected at or near the ozone measurement sites. From 1996 to 2014
144 measurements of temperature, relative humidity, wind speed, and wind direction were obtained through the
145 Danish Meteorological Institute’s weather station located within Station Nord (Jensen, 2022). From 2014
146 to 2020, measurements of temperature, relative humidity, wind speed, wind direction, and solar radiation
147 were obtained from an automatic weather station located ~44 m from the Air Observatory.

148 Observations of solar radiation only started in 2014 and input data for ML models require no
149 missing data. To overcome this absence of measurements before 2014 and extend the input dataset for the
150 ML model to 2007, we supplemented observations with ERA5 reanalysis data (Hersbach et al., 2020).
151 ERA5 output of “shortwave solar radiation downwards” was used, which is the amount of shortwave
152 downwelling solar radiation that reaches the Earth’s surface on a horizontal plane, this includes both direct
153 and diffuse radiation. This is the ERA5 equivalent of the output of a pyranometer with a radiation spectrum
154 of 0.2–4 μm (Hogan, 2015). ERA5 originally provided data as an accumulated value in J m^{-2} but was
155 converted to W m^{-2} by dividing the original values by one hour in seconds (3600). Data are on a $0.25^\circ \times$
156 0.25° spatial resolution and an hourly temporal resolution. These data were only used to substitute missing
157 data after 2014 and as a replacement for the absence of measurements before 2014 and were not included
158 in the evaluation of the statistical analysis of ODEs and meteorological variables. This approach was only
159 implemented for the machine learning model and not for the statistical analysis of meteorological variables.
160 A comparison of solar radiation measured at Villum and ERA5 data after 2014 is shown in Fig. S8. Overall,
161 ERA5 agrees quite well with observations, with a Spearman rank correlation coefficient of 0.974, although
162 ERA5 slightly underestimates with a slope of 0.881 (Fig. S8), which is common for ERA5 in the Arctic
163 (Pernov et al., 2024). ERA5 data were corrected using the slope of the observation-model comparison to
164 avoid changepoints in the time series, which could affect the results of the machine learning model.

165 **2.4. Back trajectory analysis**

166 Air mass back trajectories were calculated via the HYSPLIT trajectory model (Draxler and Hess, 1998;
167 Rolph et al., 2017; Stein et al., 2015). Trajectories of 168-hour length were calculated, arriving at 50 m
168 above ground level, for every hour from 2007 to 2019. The trajectory starting height of 50 m was selected
169 as a compromise between capturing air masses that are representative of our sampling site due to very low
170 boundary layers in the Arctic (Gryning et al., 2023) and avoiding trajectories intercepting the surface, which
171 can produce unrepresentative trajectories (Stohl, 1998). The trajectory length was chosen to avoid the
172 uncertainty associated with extremely long trajectory calculations. Trajectories were calculated based on
173 meteorological files from the NCEP/NCAR Reanalysis Data, which has a resolution of 2.5°
174 latitude/longitude (Kalnay et al., 1996). The mixed layer height for each step of each trajectory was output
175 by the HYSPLIT model. Only trajectories corresponding temporally to available ozone measurements were
176 used in this study. To analyze the geographic origins of ODEs, a concentric grid centered around the
177 location of Villum, consisting of $2^\circ \times 4^\circ$ (latitude \times longitude) grid cells, was constructed. The normalized
178 trajectory frequency for each grid cell was calculated by counting the number of trajectory steps that were



179 below the mixed layer and intersecting each grid cell. This was normalized by the total number of trajectory
180 steps that were below the mixed layer over all grid cells and multiplied by 100%.

181 For each trajectory, a surface-type footprint analysis was performed. The altitude at each step along
182 the trajectory was compared to the height of the mixed layer. That step was classified as being above the
183 mixed layer (AML) if the trajectory altitude was above this height. If the trajectory altitude was below this
184 height, then the underlying surface type (land without snow, sea, sea ice, or snow on land) was recorded
185 using a polar stereographic map of the Northern Hemisphere classified into 1024×1024 24 km grid cells.
186 The snow and ice coverage values used for the surface footprint type analysis were produced by the National
187 Oceanic and Atmospheric Association/National Environmental Satellite, Data, and Information Service
188 (NOAA/NESDIS) Interactive Multisensor Snow and Ice Mapping System (IMS) developed under the
189 direction of the Interactive Processing Branch (IPB) of the Satellite Services Division (SSD). The time
190 spent over different surfaces is expressed as a percentage of the total trajectory length.

191 2.5. Trend analysis

192 A trend analysis of trends in ODE frequency, duration, and start/end/range of ODE days for March, April,
193 and May was performed. The Mann-Kendall test was used to determine the presence of a statistically
194 significant (SS) trend (Kendall, 1948; Mann, 1945) and the Theil-Sen slope estimator was used to calculate
195 the magnitude of the trend slope (Sen, 1968; Theil, 1950) via the 3PW algorithm from Collaud Coen et al.
196 (2020). The 3PW algorithm tests for autocorrelation present in the time series, as this can affect the results
197 of the Mann-Kendall test, however, no SS autocorrelation was detected therefore these data were not
198 prewhitened.

199 2.6. Machine learning modeling

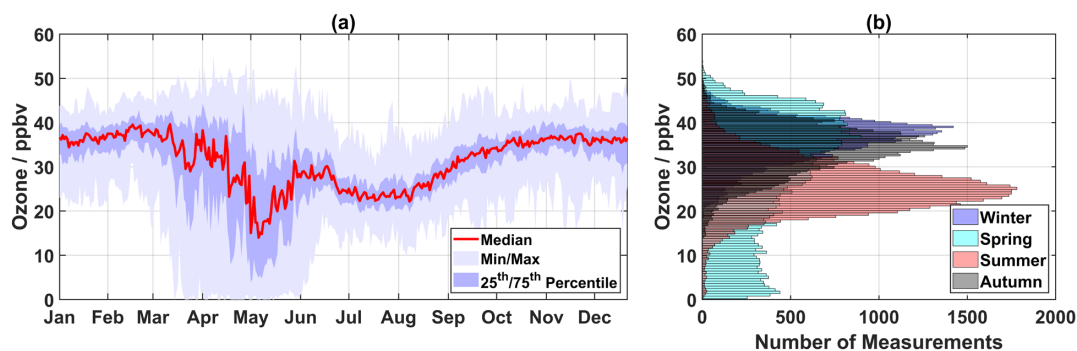
200 In this study, we utilize a supervised, binary classification form of machine learning (ML) to investigate
201 the dynamics of ODEs. The target variable used was the binary label of ODE or Non-ODE, defined as
202 ozone mixing ratios above or below 10 ppbv, respectively. The explanatory variables used in the ML model
203 were the meteorological and air mass history variables (RH, wind direction, wind speed, temperature,
204 radiation, pressure, time over snow on land, time over sea ice, and time above the mixed layer). The missing
205 data imputation, the machine learning model, hyperparameter tuning, the ML explainability approach
206 employed, and model evaluation metrics is described in the SI Text 1.



207 **3. Results**

208 **3.1. Overview of ozone and ozone depletion events**

209 The seasonal cycle of ozone mixing ratios with the daily median, minimum/maximum, and interquartile
 210 range for each day of the year is shown in Fig. 2a. During winter (December-February), ozone mixing
 211 ratios are elevated and slightly increase from January to March, displaying maximum daily median ozone
 212 values in February. During spring (March-May), ozone mixing ratios are highly variable with daily
 213 minimum values reaching 0 ppbv and maximum values observed in April. During summer (June-August),
 214 ozone mixing ratios begin to decrease in late June, remain low during July, and begin increasing in August.
 215 During autumn (September-November), ozone mixing ratios continue to increase and begin to return to
 216 wintertime values in October. A seasonal histogram of ozone mixing ratios is displayed in Fig. 2b. For
 217 winter, autumn, and summer, ozone values are normally distributed with the highest averages experienced
 218 in winter > autumn > summer. Spring experiences a non-parametric distribution and the highest and lowest
 219 observed values as explained above.



220

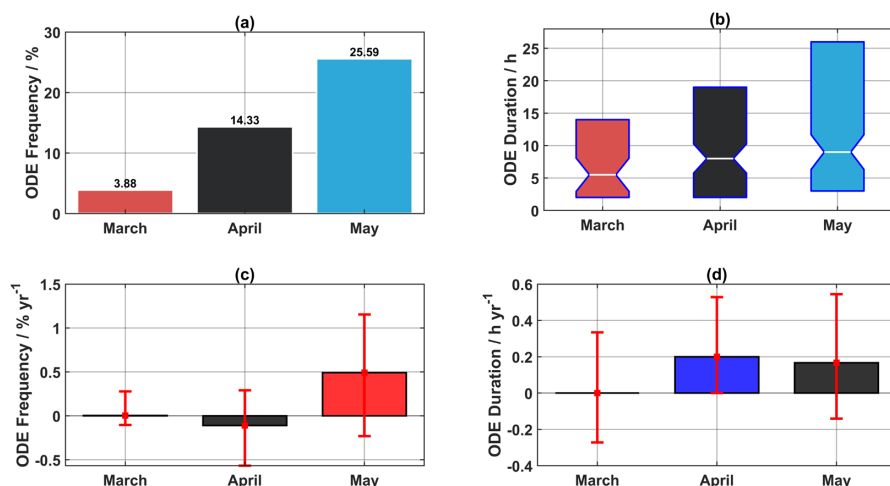
221 **Figure 2. Overview of the seasonal cycle and seasonal distribution.** (a) Seasonal ozone cycle of the daily
 222 median (red line), minimum/maximum (light blue shading), and interquartile range (blue shading) and (b)
 223 histograms of ozone by season (winter in blue: December-February, spring in cyan: March-May, summer
 224 in red: June-August, and autumn in grey: September-November).

225 An overview regarding the frequency and duration of ODEs at Villum is shown in Fig. 3a and b,
 226 respectively. ODEs were formally defined in this study as a period with ozone mixing ratio below 10 ppbv
 227 (Halfacre et al., 2014; Koo et al., 2012; Tarasick and Bottenheim, 2002; Yang et al., 2020). The frequency
 228 is calculated as the percentage of ODE hours relative to the number of available hourly observations. ODEs
 229 are most frequently observed during May, followed by April and March (Fig. 3a). The increase in the ODE
 230 frequency from March to April (10.45 %) is similar to the increase from April to May (11.26 %). The
 231 distribution (median and interquartile range) of the ODE duration for the spring months is shown in Fig.
 232 3b. The most common length of ODEs is 1-2 hours, with longer ODEs more often occurring in May. The
 233 longest ODE occurred during May and lasted 155 hours (~6.5 days). For comparison, the longest ODE
 234 observed at a ground-based Arctic station was at Alert, CA and lasted for 9 days (Strong et al., 2002). Over
 235 the central Arctic Ocean, Bottenheim et al. (2009) observed an ODE lasting from April 21 to May 23, 2007.
 236 ODEs lasting less than 8 hours occurred ~50 % of the time. ODEs lasting more than one (two) day(s)
 237 occurred 21 and 9 % of the time, respectively. Interestingly, the median of ODE duration between any of



238 the spring months is not significantly different (Fig. 3b). The median ODE duration increases from March
 239 (5.5 h) to April (8 h) to May (9 h), while the interquartile range increases more drastically from March to
 240 May (Fig. 3b). The diurnal ODE frequencies for each spring month is displayed in Fig. S2, only minor
 241 variability is displayed which is most evident during April.

242 To investigate changes in the frequency and duration of ODEs, a temporal trend analysis was
 243 performed for 1996-2019. Temporal trends of ODE frequency and duration for each month are displayed
 244 in Fig. 3c and d, respectively. The slopes of the trends are displayed as boxes (colored by p-value range)
 245 with the 95th % confidence intervals as the red error bars. For ODE frequency, no SS trends at the 95th %
 246 CL were detected, although May is SS at the 85th % CL ($p = 0.14$) with a slope of $0.49 [-0.23, 1.2] \% \text{ yr}^{-1}$.
 247 The only SS trend for ODE duration at the 95th % CL ($p = 0.039$) is during April, with an increasing trend
 248 of $0.2 [0, 0.53] \text{ h yr}^{-1}$ (slope [lower CI, upper CI]). Temporal trends in the ‘ODE season’. The first ODE was
 249 defined as the first day of the year with an ozone measurement $< 10 \text{ ppbv}$, the last ODE day was defined as
 250 the last day of the year with an ozone measurement $< 10 \text{ ppbv}$, and the range of the ODE days was defined
 251 as the difference between the last ODE day of the year and the first ODE day of the year. The results are
 252 shown in Fig. S3, and no SS trends at the 95th % CL were found.
 253



254

255 **Figure 3.** Overview of ozone depletion events including (a) bar plots of the frequency of ODEs color-coded
 256 by month, (b) boxplots of ODE duration (the white line represents the median, the colored boxes represent
 257 the interquartile range, the medians of boxes whose notches do not overlap differ with 95% confidence),
 258 (c) trends in ODE frequency, and (d) trends in ODE duration for March, April, and May. The blue, red, and
 259 black bars in (c) and (d) represent trends that are significant on the >95th, >85th, and <85th % CLs,
 260 respectively. The red error bars represent the 95th % confidence intervals of the slope. The p-values for
 261 ODE frequency in March, April, and May are 0.54, 0.75, and 0.14, respectively. The p-values for ODE
 262 duration in March, April, and May are 0.85, 0.04, and 0.41, respectively.

263



264 3.2. Statistical relationships of ODEs with meteorological variables

265 The relationships between the ODEs, ozone mixing ratios, and meteorological variables were investigated
266 by grouping the meteorological variables into bins and summing the number of ODE hours for each bin
267 which were normalized by the total number of monthly hours within the same bin and the median ozone
268 mixing ratio for each bin was calculated for each month separately. The results are shown in Figure 4, the
269 distribution (median and interquartile range) of these variables for ODEs and Non-ODEs are displayed in
270 Fig. 5, and wind roses for ODEs and Non-ODEs for the spring months are displayed in Fig. S5. It should
271 be noted that this analysis simply considers the statistical relationship between a given meteorological
272 variable and ozone/ODEs and not the causal relationship. All available data for a given meteorological
273 parameter collocated with ozone measurements was used in this analysis.

274 For RH, during March, the lowest median ozone mixing ratio and highest normalized ODE hours
275 are mainly confined in the 65-90 % range (midpoints 68-88 %) (Fig. 4a), while lower median ozone mixing
276 ratios occur at higher RHs, which are infrequent. During April and May, lower median ozone mixing and
277 higher normalized ODE hours are observed at higher RH values (75-90 %, midpoints 78-88 %) (Fig. 4a).
278 There is little difference between the distribution for RH when comparing ODEs and Non-ODEs during
279 March, while for April and May, consistently higher RH is observed during ODEs (Fig. 5a).

280 For wind direction, there is a clear effect of northerly wind directions during all spring months,
281 with the lowest median ozone mixing ratios and highest normalized ODE hours occurring in the 315°-45°
282 sector (Fig. 4b). Wind roses for each spring month show a lack of northerly winds for Non-ODE periods
283 and wind more frequently arriving from the north and northwest during ODE periods (Fig. S5).

284 For wind speed, during March, there is little effect on ozone mixing ratios and the normalized ODE
285 hours display no discernable pattern across the range of wind speeds (Fig. 4c). The distribution of wind
286 speeds shows a higher median during ODEs compared to Non-ODEs (Fig. 5b). During April, the median
287 ozone mixing ratios show little variation with wind speed although the normalized ODE hours show a
288 tendency for ODEs to occur more often at higher wind speeds (midpoints 9-15 m s⁻¹), however, these values
289 seldomly occur (Fig. 4c). The distribution of wind speeds during ODEs in April is shifted towards higher
290 values compared to Non-ODEs (Fig. 5b). During May, a clearer picture for the effect of wind speed is
291 presented; median ozone mixing ratios and normalized ODEs hours show two modes, one at low wind
292 speeds and one at high wind speeds, although it should be noted that the mode at higher wind speeds
293 (midpoints 15-18 m s⁻¹) seldomly occurs (Fig. 4c). Interestingly, during May, the distribution of wind
294 speeds was lower for ODEs compared to Non-ODEs (Fig. 5b).

295 For temperature, median ozone mixing ratios show a slight decreasing pattern for colder
296 temperatures during March and April. The normalized ODE hours showed a slight increase with colder
297 temperatures during March although for April values increased from freezing, peaked in the -25 to -20 °C
298 range (midpoint -22.5 °C), and decreased thereafter (Fig. 4d). During May, median ozone shows a stark
299 decrease with colder temperatures and the normalized ODE hours sharply increases with decreasing
300 temperatures. The -25 to -20 °C bin (midpoint -22.5 °C) displayed the lowest median ozone mixing ratios
301 and the largest normalized ODE hours during May (Fig. 4d). The distribution of temperatures is similar for
302 ODEs compared to Non-ODEs during March and April while ODEs in May experience substantially colder
303 temperatures compared to Non-ODEs (Fig. 5c).



304 For solar radiation, there are large differences in the magnitude between different spring months.
305 During March, median ozone mixing ratios (normalized ODE hours) experienced a minimum (maximum)
306 in the 100 to 150 $W m^{-2}$ range (midpoint 125 $W m^{-2}$). The distribution of solar radiation values is
307 substantially higher during ODEs in March compared to Non-ODEs and the medians are significantly
308 different on the 95th % CL (Fig. 5d). During April, median ozone mixing ratios display a decrease from the
309 lowest bin to the 50 to 100 $W m^{-2}$ bin (midpoint 75 $W m^{-2}$), afterwards they plateau until the 300 to 350 W
310 m^{-2} bin (midpoint 325 $W m^{-2}$), and finally decrease afterward and the normalized ODE hours displayed a
311 similar, yet opposite, pattern (Fig. 4e). During May, median ozone mixing ratios are consistently < 22 ppbv
312 across the range of solar radiation values (Fig. 4e). The normalized ODE hours display a maximum in the
313 0 to 50 $W m^{-2}$ bin (midpoint 25 $W m^{-2}$) although these values seldomly occur), and display similar values
314 afterward.

315 For pressure, during March and April, there is little variation in the median ozone mixing ratios
316 and normalized ODE hours, however, during May, there is a clear dependency of lower (higher) median
317 ozone mixing ratios (normalized ODE hours) with higher values of atmospheric pressure (Fig. 4f).
318 Interestingly, the distribution of pressure during ODEs is substantially higher compared to Non-ODEs for
319 each spring month, with median values being significantly different on the 95th % CL (Fig. 5e).

320 For time spent over sea ice, every spring month displays a decreasing (increasing) pattern of median
321 ozone mixing ratios (normalized ODE hours) with increasing time spent over sea ice (Fig. 4g), which
322 supports the results shown earlier for ODEs corresponding to northerly wind directions (Figs. 4b and S5).
323 Trajectories during all spring months consistently spent more time over sea ice during ODEs compared to
324 Non-ODEs (Fig. 5f).

325 For the time air masses spent over snow, no clear impact on median ozone mixing ratios is observed
326 for March and April, while May displays higher ozone mixing ratios for 90-100 % of time spent over snow
327 (Fig. 4h). During each spring month, the normalized ODE hours displays no discernable pattern over the
328 range of time spent over snow (Fig. 4h). Interestingly, the distribution of time spent over snow during ODEs
329 is consistently lower compared to Non-ODEs for each spring month and the median is significantly different
330 at the 95th % CL (Fig. 5g).

331 For time spent above the mixed layer (i.e., free troposphere), each spring month displays a similar
332 pattern, with a general tendency of decreasing (increasing) ozone mixing ratios (normalized ODE hours)
333 with less time spent above the mixed layer (Fig. 4i). The distribution of time spent above the mixed layer
334 for ODEs is consistently lower than for Non-ODEs and the median is significantly different at the 95th %
335 CL (Fig. 5h).

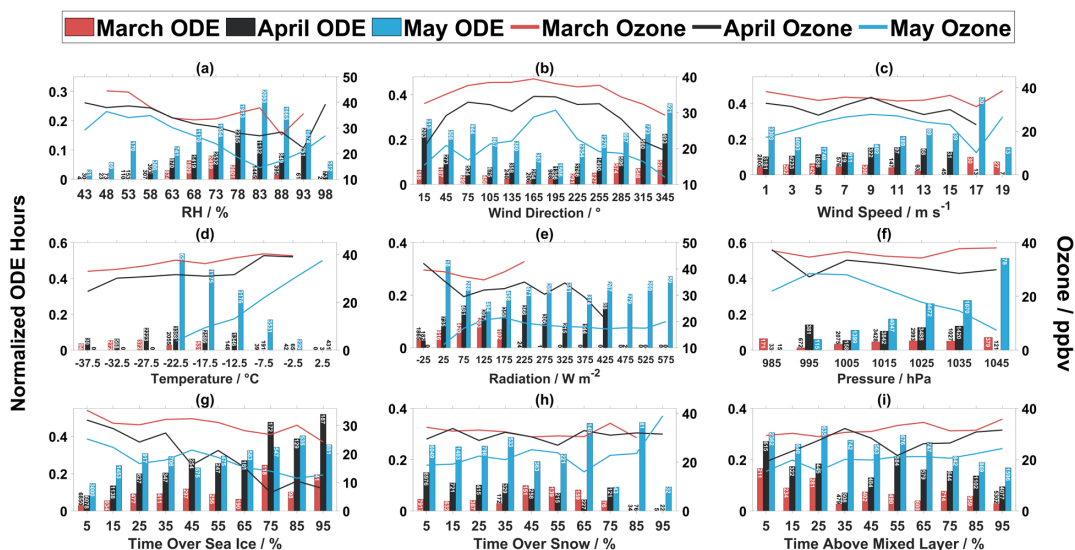
336

337

338



339

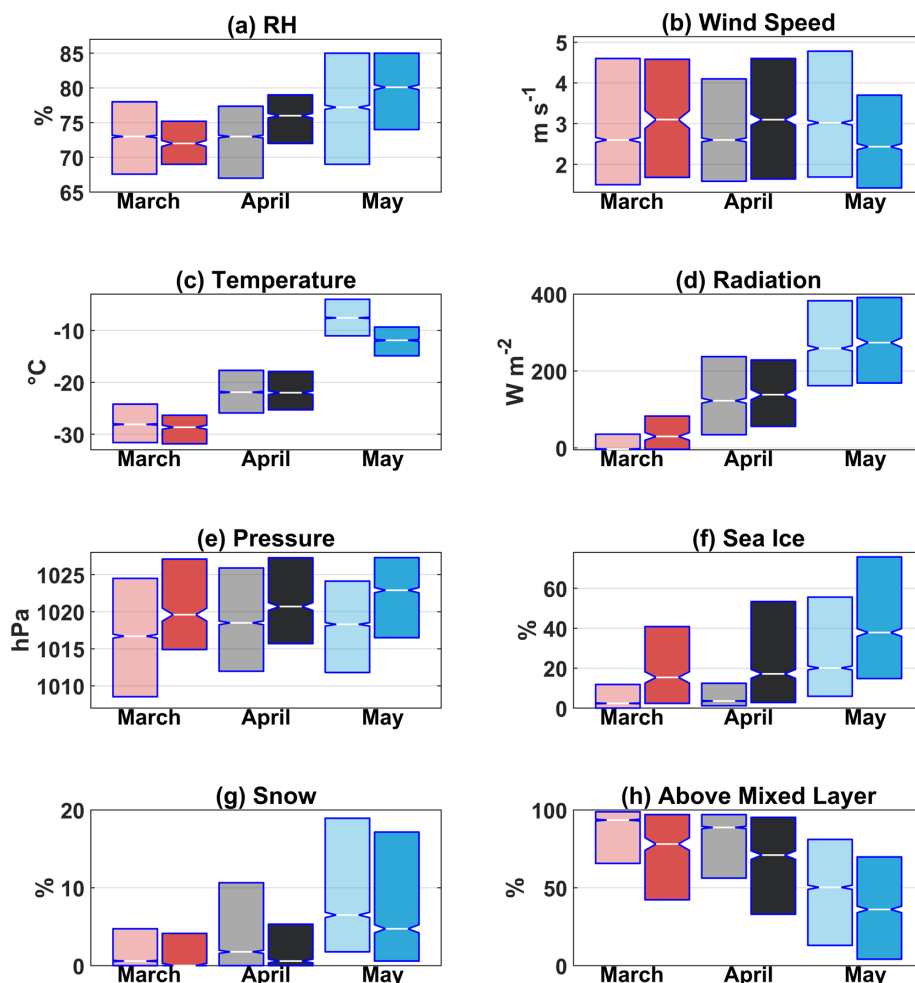


340

341 **Figure 4.** Median ozone and normalized ODE hours binned in predefined intervals of (a) RH, (b) wind
 342 direction, (c) wind speed, (d), temperature, (e) radiation, (f) pressure, time air masses spent over (g) sea ice,
 343 (h) snow on land, and (i) time above the mixed layer for March, April, and May. The number associated
 344 with each bar represents the number of total observations in that bin. All available data for each variable
 345 collocated with ozone measurements was used, resulting in different years used for each variable, with the
 346 minimum number of years included being 5 for radiation.

347

348



349

350 **Figure 5.** Distribution of meteorological and air mass history variables during the spring months for ODEs
 351 (dark colors) and Non-ODEs (light colors) including (a) RH, (b) wind speed, (c) temperature, (d) radiation,
 352 (e) pressure, (f) time over sea ice, (g) time over snow, and (h) time above the mixed layer. The line in the
 353 middle of the box represents the median, the boxes represent the interquartile range, and the medians of
 354 boxes whose notches do not overlap differ with 95% confidence. For a description of how the time spent
 355 over different surface types is calculated see the methods section. All available data for each variable
 356 collocated with ozone measurements was used, resulting in different years used for each variable, with the
 357 minimum number of years included being 5 for radiation.

358

359 3.3. Air mass history of ODEs



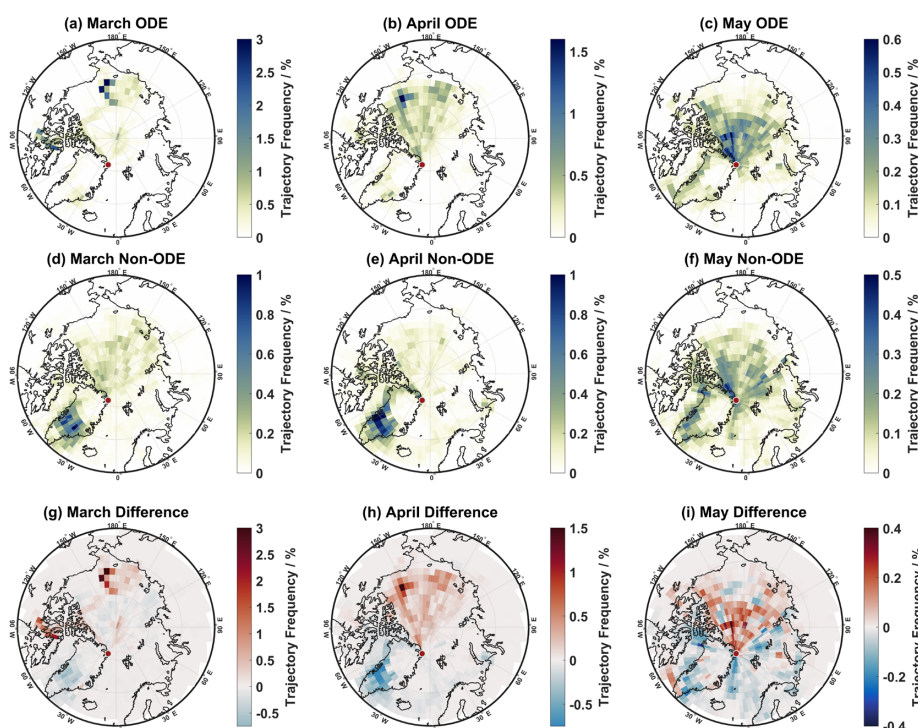
360 To understand the air mass origin of ODEs and Non-ODEs, source regions were investigated through
361 trajectory frequency maps (see Methods Sections for details). Figure 6 displays the trajectory frequency for
362 only steps below the mixed layer for ODE hours (Fig. 6a-c), Non-ODE hours (Fig. 6d-f), and the difference
363 between ODE and Non-ODE hours (Fig. 6g-i) for each spring month. Air masses arriving at Villum have
364 been shown to predominantly reside above the mixed layer (~75 %) during March and April whilst during
365 May this value decreases to ~50 % (Pernov et al., 2022), hence the smaller air mass footprint for March
366 and April. During March, the main source regions for ODEs appear to be the Chukchi Sea while for Non-
367 ODEs the main source regions are the central Arctic Ocean and Greenland (Fig. 6a and d). The difference
368 between these trajectory frequency maps during March reveals trajectories are spending relatively more
369 time over in the Chukchi Sea and Canadian Archipelago and less time over Greenland (Fig. 6g). During
370 April, ODEs are originating from the central Arctic Ocean and especially the Beaufort and Chukchi Seas
371 while Non-ODEs are arriving from the central Arctic Ocean and Greenland (Fig. 6b and e). The difference
372 between ODEs and Non-ODEs during April shows the ODEs are preferentially coming from the central
373 Arctic Ocean (Beaufort and Chukchi Seas) and are spending comparatively less time over Greenland (Fig.
374 6h). During May, ODE trajectories experience the most time over the central Arctic Ocean with a minor
375 contribution from the west coast of Greenland which is similar to the source regions of Non-ODE
376 trajectories although with increased contribution from Greenland (Fig. 6c and f). The difference between
377 May ODE and Non-ODE trajectory frequencies shows the central Arctic Ocean is the main source region
378 for ODEs and more southerly origins are related to Non-ODE trajectories (Fig. 6i).

379

380



381



382

383 **Figure 6.** Trajectory frequency maps for trajectory steps below the mixed layer for (a-c) March, April, May
 384 ODEs, (d-f) March, April, May Non-ODEs, and (g-i) difference between ODE and Non-ODE trajectory
 385 frequencies during March, April, and May at Villum (indicated by the red and white circle).

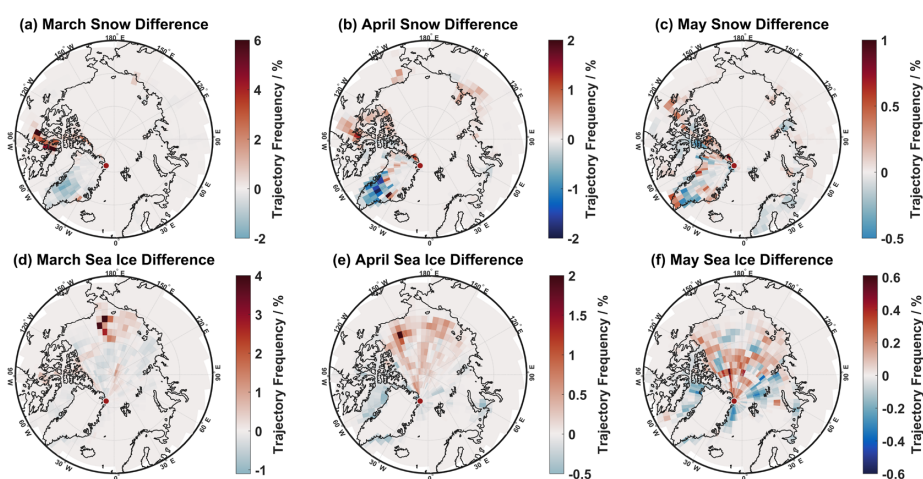
386

387 To investigate the geographic extent of the different surface types experienced during ODEs and
 388 Non-ODEs, the trajectory frequencies for steps below the mixed layer and over sea ice and snow during
 389 ODEs and Non-ODEs were also calculated, the frequencies are displayed in Figs. S6 and S7, respectively,
 390 while the difference is displayed in Fig. 7. For brevity, only the difference between ODE and Non-ODE
 391 trajectory frequencies for each spring month will be discussed.

392 During March, ODE trajectory steps over snow preferentially arrive from the Canadian
 393 Archipelago whilst they arrive less often from Greenland compared to Non-ODEs (Fig. 7a). Trajectory
 394 steps over sea ice during ODEs in March arise from the Chukchi Sea and less often arrive from the central
 395 Arctic Ocean compared to Non-ODEs (Fig. 7d). During April, ODE trajectory steps over snow display a
 396 similar pattern to March (Canadian Archipelago) although now with minor contributions from other
 397 continental regions (Greenland, Alaska, and Siberia) compared to Non-ODEs (Fig. 7b). Trajectory steps
 398 over sea ice during April preferentially arrive from the Beaufort and Chukchi Seas and less often from
 399 Baffin Bay compared to Non-ODEs (Fig. 7e). During May, ODE trajectory steps over snow preferentially



400 arrive from the Canadian Archipelago, similar to March and April, but now with increased contributions
 401 from Greenland compared to Non-ODEs (Fig. 7c). Trajectory steps over sea ice during May ODEs more
 402 often arrive from the central Arctic Ocean and less often from more southerly areas (Baffin Bay, Greenland
 403 Sea, and Barents Sea) compared to Non-ODEs (Fig. 7f). Interestingly, certain areas of the central Arctic
 404 Ocean experience more trajectory steps over sea ice during Non-ODEs compared to ODEs (Fig. 7f), this is
 405 likely due to the central Arctic Ocean being a common source area for air masses below the mixed layer
 406 during May (Fig. S7), however, the results point to the central Arctic Ocean overall being a major source
 407 region for ODEs during May.



408

409 **Figure 7.** Difference between ODE and Non-ODE trajectory frequencies for (a-c) trajectory steps below
 410 the mixed layer and over snow during March, April, May and for (d-f) trajectory steps below the mixed
 411 layer and over sea ice during March, April, May at Villum (indicated by the red and white circle).

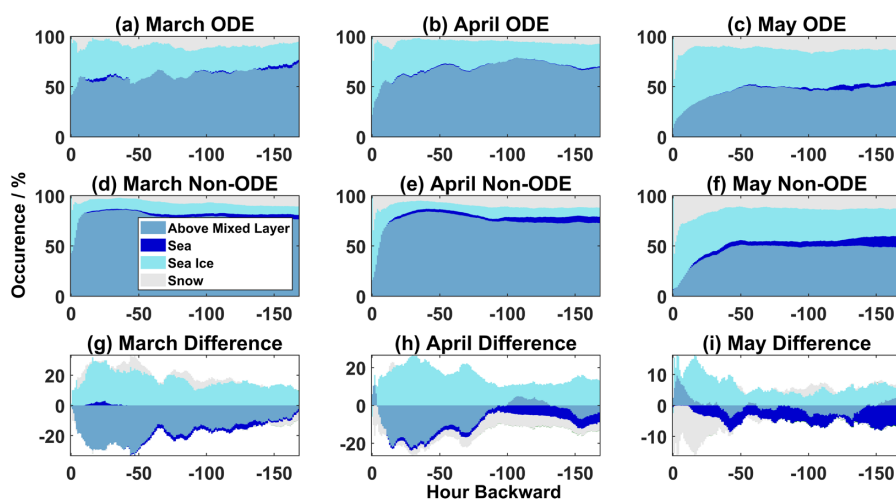
412

413 The above analysis investigated the geographic extent and surface types experienced by ODE and
 414 Non-ODE air masses, although does not give any temporal information. To further investigate the temporal
 415 relationships between ODEs and air mass history, the relative occurrence of each surface type and time
 416 spent above the mixed layer for each hourly step backward along the trajectories were calculated. Figure 8
 417 shows the results of this analysis for ODEs on the top (a-c), Non-ODEs in the middle (d-f), and the
 418 difference between ODEs and Non-ODEs on the bottom row (g-i).

419 For ODEs during March and April, air masses spend a similar amount of time above the mixed
 420 layer and over sea ice. However, during March, trajectories experience slightly more time spent over snow
 421 and the sea and during April begin their descent later along the trajectory compared to March (Fig. 8a and
 422 b). During May, ODE trajectories spend less time above the mixed layer and more time over sea ice, sea,
 423 and snow compared to March and April (Fig. 8c). For Non-ODEs during March and April a similar picture
 424 is presented, air masses spent a majority of the time above the mixed layer, followed by sea ice, snow, and



425 sea, with no contributions from land without snow and the occurrence of each surface type is relatively
 426 constant throughout the length of the trajectory until they begin their descent into the boundary layer (Fig.
 427 8d and e). For Non-ODEs during May, different air mass history conditions are presented. Air masses no
 428 longer spend a majority of the time overall above the mixed layer (45 % on average) and start to descend
 429 later along the trajectory compared to March and April (Fig. 8f). Instead, air masses experience increased
 430 time below the mixed layer and over sea ice and snow with minor increases in time spent over the sea. The
 431 time air masses spend over snow is relatively constant throughout the trajectory length until air masses start
 432 to descend. This pattern for Non-ODEs largely reflects the typical air mass history for the spring months
 433 observed at Villum (Pernov et al., 2022). The difference in the occurrence of each surface type between
 434 ODEs and Non-ODEs reveals ODE air masses experience more time over sea ice and less time above the
 435 mixed layer during March and April (Fig. 8g and h). Air masses experience more time over snow during
 436 ODEs compared to Non-ODEs when contrasting March and April, while less time over the sea is
 437 experienced during April compared to March (Fig. 8g and h). During May, the main differences between
 438 ODEs and Non-ODEs are more time over sea ice and less time over the sea and snow, interestingly, there
 439 is little difference between time spent above the mixed layer except for several hours before arrival at
 440 Villum when ODEs air masses experience more time above the mixed layer (Fig. 8i).



441

442 **Figure 8.** The occurrence of each surface type trajectories experienced in the previous 168 hours backward
 443 for (a-c) ODEs, (d-f) Non-ODEs, and (g-i) the difference between ODEs and Non-ODEs for March, April,
 444 and May. Note the differences in the y-axis scale for (g-i).

445

446 3.4. Machine Learning Modelling of ODEs

447 The statistical analysis of ODEs, meteorological variables, and air mass history variables examines the
 448 relationships between ozone/ODEs and each variable individually and does not consider interactions
 449 between, nor does it give any information about which variables are most important for ODEs. To address



450 this shortcoming and quantitatively investigate the most important variables for ODEs and how they affect
 451 ODEs, we utilized an ML model in our analysis (see Methods section for further details). The evaluation
 452 metrics of the ML for all spring months combined and individual months are displayed in Table 1. In
 453 general, the ML model can accurately reproduce ODEs over all spring months combined as evidenced by
 454 how all three metrics are close to unity (their maximum value). However, when evaluating the results on
 455 an individual monthly basis, there is an increase in model performance from March to May (Table 1), which
 456 is likely connected to the increasing frequency of ODEs from March to May, as events are easier to identify
 457 when they occur more often. The ML model is also free from over-fitting given the close agreement between
 458 the train and test sets. Overall, this ML model is sufficiently accurate, robust, and suitable for the
 459 investigation of ODEs.

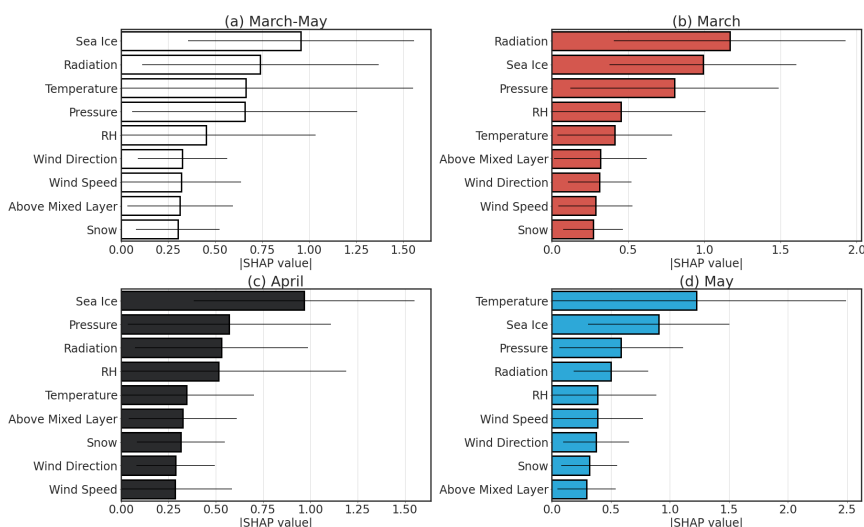
460 **Table 1.** Evaluation metrics of the ML model for the spring months, together and individually. AUC ROC
 461 stands for Area Under Curve Receiver Operating Characteristics. For each metric, the top value represents
 462 the mean 10-fold cross-validation score and the value below in parenthesis represents the standard
 463 deviation. The shaded column represents the test set evaluation metrics for clarity.

	March-May		March		April		May	
	Train	Test	Train	Test	Train	Test	Train	Test
Accuracy	0.886 (0.007)	0.870 (0.010)	0.964 (0.005)	0.955 (0.010)	0.909 (0.013)	0.870 (0.017)	0.858 (0.013)	0.809 (0.026)
Recall	0.811 (0.028)	0.738 (0.034)	0.608 (0.070)	0.504 (0.128)	0.770 (0.044)	0.642 (0.078)	0.896 (0.024)	0.856 (0.047)
AUC	0.936 (0.008)	0.905 (0.012)	0.954 (0.019)	0.911 (0.042)	0.939 (0.014)	0.865 (0.034)	0.944 (0.010)	0.897 (0.021)
ROC								

464

465 The most important variables in the ML model are explored using SHAP values (see S1 Machine
 466 learning modeling methodology for a description of SHAP values). The mean (\pm standard deviation) for
 467 each variable during all spring months and individual months is displayed in Fig. 9. The most important
 468 variables overall are time spent over sea ice, radiation, temperature, pressure, and RH, which are the top
 469 variables during all spring months combined and each month individually, although the order differs
 470 slightly (Fig. 9). While wind direction, wind speed, time spent above the mixed layer, and time spent over
 471 snow are consistently ranked near the bottom (Fig. 9). For all spring months combined, the most important
 472 variables are time spent over sea ice, radiation, temperature, pressure, and RH (Fig. 9a). During March, the
 473 most important variables are radiation, time spent over sea ice, and pressure (Fig. 9b). During April, time
 474 spent over sea ice, pressure, radiation, and RH are indicated as the most important variables (Fig. 9c).
 475 During May, the most important variables are temperature, time spent over sea ice, pressure, and radiation
 476 (Fig. 9d).

477



478

479 **Figure 9.** Overall importance of each feature in the ML model during (a) all spring months combined, (b)
 480 March, (c) April, and (d) May. The bars represent the mean of the absolute SHAP value while the lines
 481 represent the standard deviation.

482

483 While the overall importance of each variable in the ML model gives information about which
 484 variable has the biggest influence on the model output, it does not give information about the nature of the
 485 relationship between the SHAP and ambient values for each variable. Here, ambient values refer to the
 486 observed values of each variable or in other words, the input data into the ML model. To address this, we
 487 binned the ambient values of each variable into fifteen equally spaced bins and calculated the median SHAP
 488 value for each bin, as displayed in Fig. 10. A similar figure is presented in Fig. S9 which shows each month
 489 as its own subpanel with the 25th and 75th percentiles included and Figure S10 shows all spring months
 490 combined with the 25th and 75th percentiles included. Overall, the results largely agree with the results of
 491 the statistical analysis but reveal unique information about each variable during each month and how it
 492 affects the model prediction of ODEs. Notably, the presence of certain threshold ranges where the
 493 relationship between ambient and SHAP values differs above and below this range. The ranges reported
 494 here indicate the lower and upper bin limits for one or more bins.

495 Ambient values of RH are normally distributed in each month and the median SHAP values are
 496 negative for RHs below the mode of the distribution and near zero for above-average RH values (Fig. 10a).
 497 This indicates that when RH is below average it has a negative effect on the model prediction of ODEs and
 498 above average RH values have little effect on the model output.

499 Ambient values of wind speed are usually low at Villum ($< 5 \text{ m s}^{-1}$), with values rarely exceeding
 500 11 m s^{-1} , and median SHAP values are only positive for the lowest bin during April and May (Fig. 10b).
 501 With higher values of wind speed, the median SHAP values are mostly negative except for the 13-19 m s^{-1}
 502 range during May and only the 17 m s^{-1} bin during March, although these high speeds rarely occur.



503 For temperature, the ambient values are normally distributed in each month, and interestingly, a
504 threshold value for temperature is observed during all months, with negative median SHAP values observed
505 in the (-10 to -13 °C bin (midpoint of -12 °C) and values centered around zero after this bin (Fig. 10c).

506 The distribution of radiation during each month is skewed towards lower values and a threshold
507 value for positive median SHAP values is also displayed for this variable as well. At values below the 112
508 to 153 W m⁻² bin range (midpoint 133 W m⁻²) radiation makes a negative contribution to the model output
509 and at values above this bin range it contributes positively and the relationship appears to be nearly linear
510 (Fig. 10d).

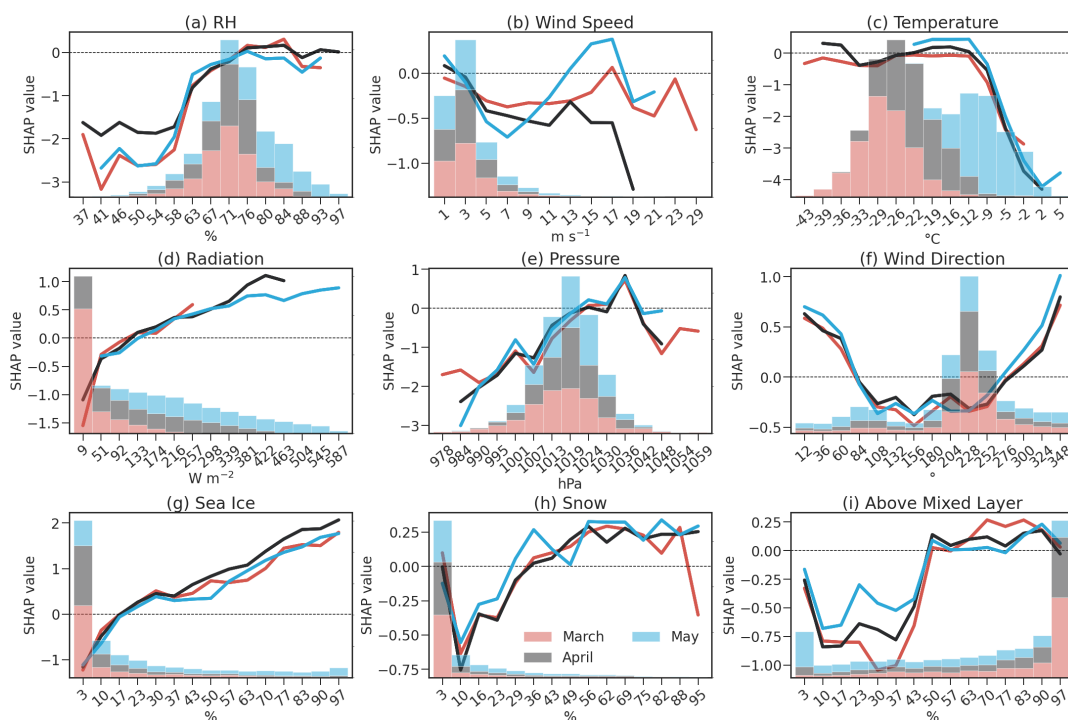
511 For pressure, the ambient values are all normally distributed in each month. Similar to RH, the
512 relationship between ambient and SHAP values is negative for below-average ambient values, although,
513 for above-average ambient values, the median SHAP value is only positive for the next several bins and
514 becomes negative at very high values of pressure (which rarely occurs though) (Fig. 10e).

515 The most common wind direction at Villum is from the southeast, as observed in previous studies
516 (Nguyen et al., 2016), although only northerly wind directions (288 ° to 72° bins) exhibit positive median
517 SHAP values (Fig. 10f). This observation is congruent with the statistical analysis of wind direction (Fig.
518 4b) and the origin of ODEs being the central Arctic Ocean (Figs. 6 and 7).

519 The distribution of time air masses spend over sea ice is skewed towards lower values for all three
520 spring months and only during May do values above 50 % occur regularly. The relationship between
521 ambient and SHAP values for time spent over sea ice is almost linear, with higher values of time spent over
522 sea ice increasing the likelihood of an ODE occurring (Fig. 10g). A threshold value for average positive
523 SHAP values for time spent over sea ice is observed at 13 to 19 % bin range (midpoint 17 %) and
524 interestingly, only after 30 % of the time spent over sea ice does the average relationship begin to differ for
525 each month, although still follows a linear pattern indicating a slightly different sensitivity towards exposure
526 to sea ice and ODEs.

527 For time spent over snow, the distribution is more skewed towards lower values when compared to
528 time spent over sea ice. The relationship between ambient and SHAP values for time spent over snow is
529 complex and non-linear (Fig. 10h). The mode of time spent over snow is also the lowest value and appears
530 to have little effect on the model output, however, the second most often occurring bin for time spent over
531 snow shows a strongly negative effect. After the third bin, SHAP values increase almost linearly and on
532 average become positive at 32-39 % bin range (midpoint 36 %) during March and April and 26 to 32 % bin
533 range (midpoint 29 %) during May. During all spring months, the SHAP values reach a plateau around 56
534 % of time spent over snow, after which, increasing time spent over snow has little effect on the model
535 prediction of ODEs (Fig. 10h). The relationship between ambient and SHAP values for time spent above
536 the mixed layer shows negative contributions until a threshold range of 46 to 53 % (midpoint 50 %) is
537 reached after which slightly positive is observed (Fig. 10i).

538



539

540 **Figure 10.** The relationships between SHAP and ambient values for (a) RH, (b) wind speed, (c),
 541 temperature, (d) radiation, (e) pressure, (f) wind direction, time air masses spent over (g) sea ice, (h)
 542 on land, and (i) time above the mixed layer for each month. Fifteen equally spaced bins were calculated for
 543 each variable, and the median of the SHAP values was computed for each bin. The value listed on the x-
 544 axis is the midpoint of each bin. The colored bars represent a histogram of the ambient values for each
 545 month. The histogram counts for each variable are omitted for clarity.

546

547



548 **4. Discussion**

549 **4.1. Overview of ozone and ozone depletion events**

550 Overall, the seasonal cycle of ozone at Villum displays a similar pattern observed at other coastal High
551 Arctic sites that experience ODEs (Barrie et al., 1988; Eneroth et al., 2007; Law et al., 2023; Schroeder et
552 al., 1998; Whaley et al., 2023), with elevated values during winter, highly variable and minimum values
553 during spring, low values during summer, and increasing values during the autumn. The elevated values
554 during winter are due to the efficient transport of anthropogenic pollution from the mid-latitudes (Stohl,
555 2006), descending air masses bringing ozone-rich air into the boundary layer (Hirdman et al., 2010), and
556 inefficient removal mechanisms (absence of sunlight, reduced dry deposition due to a stably stratified
557 atmosphere, snow coverage, and minimal wet scavenging). The minimum values observed during spring
558 are due to ozone depletion events (ODEs) (Helmig et al., 2007a; Simpson et al., 2007b) caused by reactions
559 with halogen species (Simpson et al., 2015; Yang et al., 2020). The maximum ozone values occurring in
560 April are likely due to the maximum transport efficiency of anthropogenic pollution from the mid-latitudes
561 during this period (Stohl, 2006) as well as stratospheric intrusions of dry, ozone-rich air (Helmig et al.,
562 2007b).

563 The ODE frequency and duration display an increasing pattern from March to May which is likely
564 due to air masses spending more time within the mixed layer and over sea ice coupled with increased
565 amounts of radiation, as these variables are all important for ODEs (Fig. 9) and show a similar seasonal
566 progression from March to May (Fig. 5). The geographic origin of ODEs within the mixed layer also shows
567 a seasonal progression from March to May, with sources being more distant during March and progressively
568 moving closer to Villum during April and May (Figs. 6 and 7). The ODE frequency at Zeppelin follows a
569 similar season progression with ODEs occurring more often in late spring compared to early spring (Solberg
570 et al., 1996; Zilker et al., 2023).

571 The ODE frequency and duration are increasing during May (>85th % CL) and April (>95th % CL),
572 respectively (Fig. 3). There appears to be no SS trends in the start, end, or range of ODE days for any spring
573 month (Fig. S3). SS increasing trends in ODE frequency of 0.54 [\pm 0.26] (slope [\pm 95 % CI]) have been
574 observed at Utqiagvik (formerly known as Barrow), Alaska only during March over the period 1973-2010
575 (Oltmans et al., 2012). A tendency for increasing ODE frequencies throughout the lowest level of
576 ozonesonde measurements has also been observed at Canadian Arctic sites at Alert (0.19 [\pm 0.53] % yr⁻¹,
577 1987-2020), Eureka (0.79 [\pm 0.83] % yr⁻¹, 1991-2020) and Resolute (0.60 [\pm 0.30] % yr⁻¹, 1966-2020) (Law
578 et al., 2023; Tarasick and Bottenheim, 2002). These positive trends in ODE frequencies around the Arctic
579 and the trends in ODE frequency and duration at Villum could be connected to multiple causes: an increase
580 in springtime tropospheric BrO in the Arctic as observed from satellites (Bougoudis et al., 2020), the
581 increase in Arctic sea salt aerosol due to multi-year ice being replaced with first-year ice (Confer et al.,
582 2023), changing transport patterns (Heslin-Rees et al., 2020), increasing frequency of re-freezing leads
583 (Yang et al., 2020), or increasing salinity of surface snow which release halogen compounds to the
584 atmosphere (Peterson et al., 2018; Pratt et al., 2013; Simpson et al., 2005). Further research is required to
585 elucidate the underlying causes of these trends as well as the positive trends in ozone mixing ratios observed
586 at Villum (Law et al., 2023).

587



588

589 **4.2. Dynamics of ODEs in relation to meteorological variables and air mass history**

590 Our investigation into the dynamics of ODEs at Villum, through a statistical analysis and ML modeling
591 approach, indicates that ODEs are connected to clear (high amounts of radiation), calm conditions (cold
592 temperatures, high pressures, and low wind speeds) with air masses arriving from a northerly direction
593 having experienced surface contact with sea ice (northerly wind directions and air masses experiencing a
594 high amount of time over sea ice in the central Arctic Ocean). Our ML model revealed the most important
595 variables are similar throughout each month (time over sea ice, radiation, temperature, and pressure) but
596 exhibit different orders (Fig. 9). This indicates that the ML model can discern the overall conditions leading
597 to ODEs but also reveal distinct circumstances in each month. For instance, the time air masses spent over
598 sea ice was consistently among the top variables for each month, which likely indicates the release of
599 halogen species from sea ice (or snow on top of sea ice) is a key condition for the observation of ODEs at
600 Villum. During March, the most important variable is radiation, whilst during May it is temperature.
601 Interestingly, these two variables (radiation and temperature) are often limited during these months (March
602 and May), with low values of radiation during March and temperatures closer to 0 °C during May (Fig. 5d
603 and c, respectively). In the following paragraphs, we discuss each variable's relation to ODEs for each
604 spring month through our statistical analysis, ML modeling, and back-trajectory source regions.

605 Solar radiation is required for the photolysis of molecular halogen species (Peterson et al., 2018;
606 Pratt et al., 2013; Raso et al., 2017; Wang et al., 2019). The results presented in Fig. 4e show that ODEs
607 can occur across all values of radiation during April and May whilst March shows more clear dependency
608 and only during March were solar radiation medians significantly different during ODEs and Non-ODEs
609 (Fig. 5d) and solar radiation appears to be a limiting factor. During April and May, sunlight is omnipresent,
610 therefore a clear lack of dependency for ozone mixing ratios and normalized ODE hours with radiation is
611 not unexpected. This is supported by the high importance of radiation in the ML model during March
612 compared to April and May (Fig. 9b). The results from the statistical analysis suggest that while the
613 presence of solar radiation is required, the intensity is not a limiting factor for the occurrence of ODEs.
614 However, the relationships between ambient and SHAP values of radiation indicate there is a near-linear
615 relationship (Fig. 10d), which highlights the added value of ML modeling. Alternatively, this could be due
616 to ODEs resulting from the advection of previously depleted air masses, and in situ solar radiation
617 measurements are not indicative of conditions along the trajectory path or in regions where depletion is
618 occurring (Bottenheim and Chan, 2006; Halfacre et al., 2014). It should be noted that solar radiation
619 measurements started in the autumn of 2014 thus only five years of data are included in the statistical
620 analysis while the ML model was supplemented with radiation from ERA5 (see Methods), this could also
621 contribute to the discrepancy between analysis methods.

622 Cold temperatures have been shown to be an important factor influencing ODEs (Simpson et al.,
623 2007b, 2015), indeed frozen heterogeneous surfaces can lead to the release of bromine, which is known
624 from studies using reanalysis products (Seo et al., 2020; Zilker et al., 2023), laboratory experiments (Abbatt
625 et al., 2012; Halfacre et al., 2019), and mesocosm/field studies (Gao et al., 2022; Pöhler et al., 2010; Pratt
626 et al., 2013; Swanson et al., 2020). Observational evidence has shown halogen activation ceases at above-
627 freezing temperatures (Burd et al., 2017; Jeong et al., 2022). While several studies have reported a
628 temperature dependency of ODEs (Koo et al., 2012; Pöhler et al., 2010; Tarasick and Bottenheim, 2002;



629 Zeng et al., 2006), other studies have not (Halfacre et al., 2014; Jacobi et al., 2010; Neuman et al., 2010;
630 Solberg et al., 1996). Any relationship between ODEs and temperature is likely a result of air masses having
631 surface contact with the cold Arctic Ocean before arriving at Villum, where cold temperatures aid in the re-
632 freezing of leads as well as formation of sea ice and frost flowers (Kaleschke et al., 2004; Yang et al., 2020),
633 all of which are known halogen sources. Cold temperatures could also indicate the presence of a temperature
634 inversion, which traps oxidants and ozone near the surface and inhibits vertical mixing, which replenishes
635 ozone and terminates ODEs (Moore et al., 2014). Temperature has the greatest influence on ODEs during
636 May (Fig. 9d), which is the only month which regularly experiences temperatures above the threshold range
637 of -10 to -13 °C found through our ML model analysis (Figs. 4, 5, and 10). Similar to radiation, the
638 temperature used in this analysis does not necessarily represent the temperature where ozone depletion
639 occurred, although temperature is usually highly correlated to previous days' measurements and therefore
640 gives a good indication of the temperature upwind of Villum. Therefore, this temperature threshold range
641 should not be interpreted as absolute but rather as the existence of a threshold where temperature has little
642 effect below and a negative contribution to ODEs above. This observation could help explain the
643 contradictory evidence about a temperature dependence for ODEs. Depending on the local conditions of
644 the measurement site, ODEs might be observed at temperatures below this threshold range (which would
645 indicate no relationship) or above this threshold range (where ODEs show a negative relationship with
646 temperature). This threshold range would be site specific and emphasizes the need for Pan-Arctic
647 assessments of the temperature dependency of ODEs.

648 Above-average values of RH are revealed to be conducive to ODEs through our statistical and ML
649 model analysis (Figs. 4, 5, and 10). A relationship between RH and ODEs has not been reported in the
650 literature before (to the authors' knowledge) and the physical mechanism behind this observation remains
651 unclear. We hypothesize that the higher normalized ODE hours (Fig. 4a) and positive SHAP values (Fig.
652 10a) for above-average RH values during ODEs are likely connected to air masses spending time over the
653 central Arctic Ocean where RH would be higher due to the cold temperatures and escape of water vapor
654 through open leads and polynya (Bintanja and Selten, 2014; Boisvert et al., 2015). The lower values of
655 normalized ODE hours (Fig. 4a) and negative SHAP values (Fig. 10a) for below-average RH could also be
656 related to drier air masses having experienced higher altitudes during transport to Villum, which are ozone-
657 rich and less influenced by the surface (Moore et al., 2014).

658 Northerly wind directions are more common during ODEs compared to Non-ODEs (Fig. S6),
659 corresponding to low ozone values, high normalized ODE hours, and positive SHAP values (Figs. 4b and
660 10f). A similar observation was made at Utqiaġvik/Barrow, AK, for low ozone mixing ratios showing a
661 clear minimum when wind arrived from northerly directions (Helmig et al., 2012). Halfacre et al. (2014)
662 used buoy measurements of ozone and air mass direction to show that northerly directions were dominating
663 but easterly and westerly directions also made a contribution, showing that in the central Arctic Ocean wind
664 direction has less of an influence due to the omnidirectional presence of sea ice. These observations are
665 directly related to the presence of sea ice in a northerly direction relative to these land-based stations (Fig.
666 1).

667 Wind speed can have dual effects on ozone variability, with low wind speeds corresponding to a
668 stable boundary layer where reactants are confined to a small volume and high wind speeds generating
669 blowing snow, which acts as a source of reactive halogen species as well as favoring advection of air masses
670 previously depleted in ozone (Jones et al., 2009; Swanson et al., 2020). The distribution of wind speeds



671 during March and April were consistently higher for ODEs compared to Non-ODEs, this relationship is
672 reversed for May (Fig. 5b) but in all months relatively low wind speeds prevailed ($< \sim 3 \text{ m s}^{-1}$). Our statistical
673 analysis revealed no relationship during March, a tendency for high normalized ODE hours during April
674 (although little effect on ozone mixing ratios), and two modes during May (one at low and one at high wind
675 speeds) (Fig. 4c). The ML model also showed a similar relationship during May (positive SHAP values at
676 low and high wind speeds), although these high wind speeds did not occur very often. Overall, wind speeds
677 are usually low at Villum (Figs. 4c, 5b, and 10b; Nguyen et al. (2016)). Low ozone mixing ratios concurrent
678 with low wind speeds have also been observed at Utqiaġvik/Barrow, AK, at Zeppelin Observatory on
679 Svalbard, and from buoy measurements in the Arctic Ocean (Bottenheim et al., 2009; Halfacre et al., 2014;
680 Helmig et al., 2012; Solberg et al., 1996). Conversely, enhanced BrO events at Zeppelin, Eureka, and Alert
681 as well as for the Arctic region have been connected to high wind speeds, mostly likely related to stormy
682 conditions that generate blowing snow (Seo et al., 2020; Swanson et al., 2020; Zhao et al., 2016; Zilker et
683 al., 2023). The results of our statistical and ML model analysis suggest that ODEs at Villum occur mainly
684 under stable conditions with low wind speeds and are likely not connected to the generation of halogen
685 species through blowing snow and Arctic cyclones. Only during May does high wind speeds regularly make
686 a positive contribution to the model output, and the magnitude of this contribution is small (Fig. 10b).

687 Distributions of pressure are consistently higher for ODEs compared to Non-ODEs during each
688 spring month (Fig. 5e) and above-average pressure is related to the occurrence of ODEs as shown through
689 our statistical analysis (Fig. 4f) and our ML model (Fig. 10e). High-pressure systems could indicate the
690 presence of a stably stratified lower troposphere and low-pressure systems could signal the passage of
691 frontal systems which are conducive for strong vertical mixing (which bring ozone rich down from aloft)
692 and a break up of inversion layers (Hopper et al., 1998; Jacobi et al., 2010; Simpson et al., 2015). Ozone
693 and atmospheric pressure have been shown to be anti-correlated during spring in the Arctic Ocean (Jacobi
694 et al., 2010). Conversely, low pressures have been associated with ODEs at Zeppelin (Zilker et al., 2023)
695 and BrO enhancement events over the Arctic region (Blechschmidt et al., 2016; Seo et al., 2020) and at
696 Eureka, CA (Zhao et al., 2016), where they were related to polar storms and blowing snow generation of
697 reactive halogens. The pressure dependence of ODEs found at Villum is congruent with the relationship
698 for wind speed (Fig. 10b) and further suggests that Arctic cyclones and blowing snow do not have an
699 important effect on ODEs at Villum. Furthermore, very high values of pressure are likely associated with
700 descending air masses from aloft which are often enriched in ozone and contain few sources of halogen
701 species (Simpson et al., 2007b; Peterson et al., 2015; Swanson et al., 2020), which could explain the
702 negative SHAP values at high values of pressure although it should be noted that these values do not occur
703 often (Fig. 10e).

704 Heterogeneous, photochemical reactions on the snowpack have been demonstrated to be a source
705 of reactive halogen species (Pratt et al., 2013; Raso et al., 2017; Peterson et al., 2018; McNamara et al.,
706 2020), as well as the generation of blowing snow at high wind speeds and subsequent release of reactive
707 halogens (Jones et al., 2009; Marelle et al., 2021; Chen et al., 2022; Swanson et al., 2022; Zilker et al.,
708 2023). Air masses spend little time over snow during each spring month (Fig. S4g) and on average ODEs
709 actually experience less time over snow compared to Non-ODEs (Fig. 5h). Non-ODEs experiencing more
710 time over snow is likely tied to the different regions of snow contact for Non-ODEs (southern half of
711 Greenland) (Fig. S6d-f), while source regions of air mass contact with snow during ODEs are consistently
712 in the Canadian Archipelago and Greenlandic coasts during the spring months (Fig. S6a-e). The Canadian
713 Archipelago has been demonstrated to be a hotspot for BrO enhancements (Bognar et al., 2020; Bougoudis



714 et al., 2020; Seo et al., 2020), which has been connected to low pressure and high wind speeds suggesting
715 blowing snow to be a source of halogen species in this region. Contributions from other continental regions
716 (Alaska and Siberia) to snowpack exposure only appear in April (Fig. 7b), which could reflect the greater
717 extent of the polar dome during this month (Stohl, 2006). Snowpack located on the west coast of Greenland
718 only appears to contribute to ODEs during May (Fig. 7c), this could be related to air masses spending more
719 time below the mixed layer during May compared to other months (Fig. 5h). Our statistical analysis
720 suggests there is no clear dependency of ozone mixing ratios and normalized ODE hours on varying
721 amounts of times spent over snow (Fig. 4h). Our ML model revealed that low values of time spent over
722 snow contributes negatively whereas after a threshold range of 26-39% (depending on the month), time
723 spent over snow makes a small positive contribution to the model output that varies little with increasing
724 values (Fig. 10). This is supported by the back-trajectory analysis, which showed that ODE air masses are
725 not preferentially experiencing more time over snow during any particular point along the trajectory length
726 compared to Non-ODEs (Fig. 8g-i). High amounts of time spent over snow are uncommon during each
727 spring month, therefore, it is difficult to assess the importance of snowpack mechanisms on ozone depletion
728 at Villum. Generation of halogen species in the Canadian Archipelago, either through snowpack emissions
729 or blowing snow at higher wind speeds, appears to consistently make a minor influence on ODEs during
730 each spring month.

731 Sea ice sourced halogens have been indicated to be responsible for halogen generation necessary
732 for ozone depletion (Simpson et al., 2007b; Halfacre et al., 2014; Simpson et al., 2015; Burd et al., 2017;
733 Yang et al., 2020; Marelle et al., 2021; Brockway et al., 2024). The amount of time spent over sea ice
734 increases from early to late spring (Fig. S4f) and ODEs experience higher values during each spring month
735 compared to Non-ODEs (Fig. 5f). Our statistical analysis displays increased (decreased) normalized ODE
736 hours (ozone mixing ratios) with higher values of time spent over sea ice (Fig. 4g), which is congruent with
737 the ML model showing higher SHAP values for more time spent over sea ice. This relationship is linearly,
738 positive and on average becomes positive after the 13 to 19 % threshold range (Fig. 10g). Indicating that
739 air masses need to spend only a fraction of time over sea ice for it to increase the probability of observing
740 an ODE at Villum. The back-trajectory analysis shows that ODE air masses experience more time over sea
741 ice closer to the measurement site compared to Non-ODEs (Fig. 8g-i). It has been found that ODEs can be
742 the result of the transport of previously depleted air masses, where ozone depletion was occurring relatively
743 far (several hundred kilometers) from the observation point (Halfacre et al., 2014; Tarasick and Bottenheim,
744 2002; Yang et al., 2020). As the spring progresses from March to May, it appears that the main ODE
745 geographic source regions for sea ice contact are moving closer to Villum each month (Fig. 7d-f). During
746 March, ODEs are initiated over the Chukchi Sea, which is usually covered by first-year sea ice (FYI) (Fig.
747 1). During April, ODEs are initiated over the Beaufort and Chukchi Seas but also over the central Arctic
748 Ocean, which represents a mix of FYI and multi-year sea ice (MYI). During May, ODEs occur in closer
749 proximity to Villum, mainly arriving from the central Arctic Ocean, which contains the highest
750 concentration of MYI. This source region analysis is supported by the wind sector/speed analysis, which
751 displays a northerly wind direction dependency for ODEs during each spring month (Figs. 4b, S5, and 10f).
752 During March and April, wind speeds during ODEs are consistently higher compared to Non-ODEs whilst,
753 during May, wind speeds are lower (Fig. 5b). This could indicate that in March ODEs likely result from the
754 transport of ozone-depleted air masses from FYI regions, April experiences a mixture of transport-related
755 ODEs and ODEs occurring closer to Villum from FYI and MYI regions, whilst May ODEs occur in
756 proximity to the measurement site, arriving mainly from regions with MYI but also with influences from



757 FYI in the central Arctic Ocean. This is supported by Herrmann et al. (2022), who suggested that MYI
758 makes important contributions to ozone depletion at Villum, and by Marelle et al. (2021) who showed that
759 both snowpack emissions and blowing snow can contribute to ozone depletion, although sea ice surfaces
760 were responsible for regional ozone depletion and halogen activation. It should be noted that this analysis
761 is based on trajectory frequency maps and average sea ice age over the observation period and a more
762 detailed investigation of sea ice age would help elucidate the exact contribution of FYI and MYI on ODEs.

763 While this and previous work point towards ODEs being a surface-related process through the
764 generation of reactive halogen species from sea-ice and snowpack mechanisms, the activation of halogen
765 species on aerosol particles aloft has also been demonstrated (Bognar et al., 2020; Peterson et al., 2017;
766 Seabrook and Whiteway, 2016; Solberg et al., 1996). A general feature of the distributions for ODEs and
767 Non-ODEs when progressing from March to May is that trajectories spend increasingly less time above the
768 mixed layer (Fig. 5h). Our statistical analysis indicates that, in general, ODEs are more likely to occur and
769 ozone mixing ratios are more likely to be lower when air masses spend more time near the surface (Fig. 4i).
770 Although ODE trajectories spend less time above the mixed layer compared to Non-ODEs trajectories
771 (Figs. 5h and 8g-i), they are still spending a considerable amount of time aloft as the median time spent
772 above the mixed layer only drops below 50 % during May (Fig. 5h). The recycling of halogen species on
773 lofted aerosol particles could explain the ODEs experiencing a significant amount of time above the mixed
774 layer, this would be especially relevant for the earlier spring months (March and April) given the burden of
775 acidic, tropospheric aerosols (i.e., Arctic Haze) is greatest during these months (Flyger et al., 1980; Heidam
776 et al., 1999, 2004; Nguyen et al., 2013, 2016) and the increased amount of time air masses spend above
777 mixed layer during these months. Our ML model revealed on average a positive contribution at > 46 to 53
778 % threshold range of time spent above the mixed layer (Fig. 10i). A physical explanation for our ML results
779 for the time above the mixed layer SHAP values could be that ozone is initially depleted within the boundary
780 layer, depleted air masses are lifted and remain depleted either through inhibited mixing with ozone rich
781 air, decreasing mixed layer height with frequently occurring surface temperature inversions, or halogen
782 recycling on acidic aerosol particles. This could also be due to the time spent over mixed layer being
783 calculated over the entire trajectory length and therefore is not time resolved. It is also important to note
784 that SHAP values represent how well these variables explain the behavior of our target variable in our ML
785 model and not how well the input variables explain the behavior of our target variable in the natural
786 environment.

787 To understand the conditions leading to a correct model prediction for the input variables and
788 investigate the cause of the relationship between ambient and SHAP values for time spent above the mixed
789 layer, we calculated the distribution of ambient and SHAP values for correctly and incorrectly labeled
790 observations of ODEs and Non-ODEs for all spring months combined and each month individually. The
791 results for the ambient and SHAP value distributions are displayed in Fig. S11 and S12, respectively. The
792 variables with the largest differences in the distribution of correct vs incorrect ODEs are time spent above
793 the mixed layer, time spent over sea ice, and radiation, whilst RH, time spent over snow, wind direction,
794 and wind speed showed little differences (Fig. S11). The variables with the largest differences are also
795 indicated as the most important variables and variables with little differences were shown to be the least
796 important (Fig. 10), except for time above the mixed layer. Temperature displays a large difference between
797 correct and incorrectly labeled ODEs when evaluating all spring months combined but when analyzing
798 individual spring months, this difference is diminished, which likely is a result of the seasonal progress of
799 warmer temperatures later in the spring (Fig. 5c). The distributions for SHAP values between correctly and



800 incorrectly labeled ODEs shows that time spent over sea ice SHAP values experienced the largest difference
801 for all spring months combined and each individual month (Fig. S12). Other variables showing large
802 differences in the distribution of SHAP values include pressure, temperature, radiation, and wind direction.
803 Time spent above the mixed layer did not show large differences between correctly and incorrectly labeled
804 ODEs, likely a result of the small magnitude of the SHAP values for time spent above the mixed layer,
805 indicating this variable does not largely contribute to the model output (Fig. 9), therefore, while this
806 relationship is counterintuitive it is not affecting the accurate prediction of ODEs in our ML model. The
807 large differences between the distribution of time spent above the mixed layer for correctly vs incorrectly
808 labeled ODEs could be the underlying cause of the counterintuitive relationship between ambient and
809 SHAP values for this variable displayed in Fig. 10, this could also be a result of ODE trajectories
810 experiencing a majority of time above the mixed layer further back along the trajectory length (Fig. 8a-c).
811 Other factors that could contribute to this relationship include the length of the back-trajectory (trajectories
812 could be too long and experience comparatively more time above the mixed layer further backward),
813 misrepresentation of the mixed layer height from the HYSPLIT model (too low of a mixed layer height
814 would result in a larger fraction of air masses above this altitude), the uncertainty of HYSPLIT increases
815 proportionately with the trajectory length, and the starting altitude of the back-trajectories being too high
816 (higher starting altitude would result in a larger fraction of air masses residing above the mixed layer).
817 Proper representation of air mass history therefore is an important aspect of evaluating ODEs and other
818 atmospheric phenomena. Overall, this shows the ability of ML to identify the appropriateness of input
819 variables for modeling atmospheric phenomena and suggests that the importance of time spent above the
820 mixed layer and time spent over sea ice might be over- and under-estimated, respectively, as the ML model
821 mis-characterizes their effect on ODEs.

822

823



824 5. Summary and Outlook

825 Our results show that ODEs occur every spring with an increasing frequency from early to late spring. This
826 seasonal pattern is the result of higher amounts of radiation, air masses spending more time within the
827 mixed layer and over sea ice, and source regions for air mass contact with sea ice (and thus ozone depletion)
828 moving closer to Villum from March to May. ODE duration and frequency displayed positive trends during
829 April and May, respectively, however, we have low confidence in the frequency trend. Positive trends in
830 ODE frequency at other Arctic sites suggest this is a Pan-Arctic phenomenon. Possible causes for the
831 increasing duration and frequency of ODEs include increasing FYI, BrO, saltier snowpack, changing
832 transport patterns, and increased occurrence of refreezing leads.

833 ODEs are likely to occur during clear (high amounts of radiation), calm (cold temperatures, high
834 pressure, low wind speeds) conditions with air masses arriving from northerly wind directions with sea ice
835 contact (high time over sea ice, high RH). Time spent over sea ice, radiation, temperature, and pressure are
836 shown to be the most important factors affecting ODEs. The most important variable affecting ODEs
837 changes as spring progresses are radiation during March, sea ice during April, and temperature during May.
838 During March and May, radiation and temperature are often the limiting factors, with smaller amounts of
839 radiation observed during March and warmer temperatures observed during May. The source regions for
840 ozone depletion also change as spring progresses. During March, sea ice (likely FYI) in the Chukchi Sea is
841 the main source region. During April, a mix of FYI and MYI in the Chukchi and Beaufort Seas and the
842 central Arctic Ocean are the main source regions for ODEs. During May, sea ice (likely a mix of FYI and
843 MYI) in the central Arctic Ocean is the main ODE source region. Snowpack emissions from the Canadian
844 Archipelago make a consistent yet minor contribution during each spring month. The back-trajectory and
845 wind speed analysis indicate that ozone depletion occurs upwind of Villum during early spring and moves
846 progressively closer towards Villum during late spring.

847 We show that ODEs can be accurately predicted using ML modeling, with physically interpretable
848 results. We also show that ML can be a useful tool for investigating atmospheric phenomena, by quantifying
849 the importance of each variable, identifying threshold ranges for positive contributions, and investigating
850 the appropriateness of input variables. Of the sources leading to halogen emission (sea ice, snowpack, and
851 recycling on aerosol particles aloft), our results suggest that emissions from sea ice are the most important.

852 While this work has made progress in understanding the dynamics of ozone depletion in the Arctic,
853 further investigation is warranted. Recent research has shown that ozone mixing ratios are increasing around
854 the Arctic (Christiansen et al., 2022, 2017; Cooper et al., 2020; Law et al., 2023), coupled with the positive
855 trend in Pan-Arctic ODE frequencies and the positive trend in ODE duration observed in this study, suggest
856 that the factors controlling ozone variability are being altered and warrant a detailed investigation into the
857 underlying causes. Recently, iodine has been shown to be as important as bromine to ozone destruction in
858 the central Arctic Ocean (Benavent et al., 2022), further studies investigating this discovery at Pan-Arctic
859 stations are needed to evaluate iodine's role in ozone depletion over the entire Arctic region, ML could aid
860 in this task. Future studies investigating ozone and ODE dynamics would benefit from the incorporation of
861 direct measurements of halogen species to investigate different chemical regimes of ozone destruction,
862 which will help predict the response of springtime ozone dynamics in a future climate. Direct halogen
863 measurements will also help elucidate the cause of ODE initiation, duration, and termination as well as
864 determine if ODEs are the result of the transport of already depleted air masses or if ODEs are occurring



865 locally at Villum. Incorporating time-resolved air mass history variables and air-mass exposure to first- and
866 multi-year ice sea ice concentration would help clarify the role of different cryosphere environments in
867 ozone destruction. Future studies should also consider the vertical structure of the lower atmosphere (i.e.,
868 the mixed layer height and its variability) when initializing trajectory calculation as this can have an effect
869 on the air mass history. While this and many other studies investigate ozone at the surface, the radiative
870 forcing of ozone is largely determined by its vertical distribution (Lacis et al., 1990; Stevenson et al., 2013),
871 therefore, studies investigating the vertical as well as the horizontal distribution are needed.

872 The added value of ML modeling over classical statistical analysis is highlighted by identifying
873 variable importance, quantitative relationships, threshold ranges, and input variable deficiencies. While a
874 statistical analysis can qualitatively identify relationships, ML can identify synergistic efforts regarding
875 interactions between variables, indicating the right mix of conditions is necessary for ODEs to occur – high
876 sea ice contact, high amounts of radiation, cold temperatures, and high pressure. The ML methodology
877 could be applied to other Arctic stations, either individually or utilizing multi-station (e.g., ground-based,
878 ship-based, buoys) merging techniques for Pan-Arctic modeling of ODEs, where the environmental drivers
879 of ODEs could be investigated from a geographic perspective. This would be especially pertinent for
880 measurements performed over sea ice, where the actual ozone destruction is likely occurring. ML modeling
881 could also be used to investigate other atmospheric phenomena such as AMDEs and BrO enhancement
882 events and for bias-correcting chemical transport models.

883 The results from our ML model largely agree with our statistical analysis and are physically
884 meaningful/interpretable but also reveal threshold ranges for certain variables that are not evident otherwise
885 and can help predict the response of ODEs in a future climate. Rising temperatures in the Arctic (Rantanen
886 et al., 2022) could affect ODEs through earlier onset of melt days by ceasing halogen emissions. The
887 temperature relationship displayed in this study (Fig. 10c) indicates that rising temperatures would have the
888 biggest effect in May and would not start to negatively affect ODEs until they rise above the threshold
889 range of -10 to -13 °C. Arctic sea ice is rapidly diminishing (Kwok, 2018; Stroeve and Notz, 2018) and the
890 Arctic Ocean is projected to be completely ice-free during summer in the coming decades (Kim et al., 2023;
891 Notz and Community, 2020), which will have profound effects on ODEs (Simpson et al., 2007b, 2015).
892 Retreating sea ice would have a major effect on ODEs when sea ice loss is propagated into the springtime
893 and these effects would be most profound in May. Conversely, retreating sea ice would also increase sea
894 salt aerosol emission through increased areas of open water, which is a source of bromine emission and
895 recycling, therefore the competing effects of sea ice retreat require further investigation through coupled
896 cryosphere-atmosphere modeling approaches. Changes in cloud cover, especially low-level liquid
897 containing clouds, would affect the amount of solar radiation reaching the surface. Previous studies have
898 presented evidence for positive and negative trends in low cloud cover for the Arctic region (Boccolari and
899 Parmiggiani, 2018; Jenkins and Dai, 2022; Lelli et al., 2023; Sviashchennikov and Drugorub, 2022; Wang
900 et al., 2021). Increases in cloud cover would affect the amount of radiation received at the surface, which
901 would affect ODEs mainly in March when radiation is lower compared to the later spring months. How the
902 Arctic and the nature of ODEs evolve with climate change remains an open question and should be the
903 focus of future research endeavors.

904



905 **Financial Support**

906 This research has been financially supported by the Danish Environmental Protection Agency and the
907 Danish Energy Agency, with continuous funding over the years from the “Danish Program for Arctic
908 Research” and ERA-PLANET (The European Network for observing our changing Planet) projects, as well
909 as by iGOSP, iCUPE, and finally by the Graduate School of Science and Technology, Aarhus University.
910 J.B.P received funding from the Swiss Data Science Center project C20-01 Arctic climate change:
911 exploring the Natural Aerosol baseline for improved model Predictions (ArcticNAP). This project received
912 additional funding from the Ingvar Kamprad Chair funded by Ferring Pharmaceuticals and held by Prof.
913 Julia Schmale from École Polytechnique Fédérale de Lausanne (EPFL).

914 **Acknowledgments**

915 Villum Foundation is gratefully acknowledged for financing the establishment of Villum Research Station.
916 Thanks to the Royal Danish Air Force and the Arctic Command for providing logistic support to the project.
917 Christel Christoffersen, Bjarne Jensen, Martin Ole Bjært Sørensen, Claus Nordstrøm and Keld Mortensen
918 are gratefully acknowledged for their technical support. The Danish Meteorological Institute (DMI) is
919 acknowledged for measurements from Station Nord (Jensen, 2022). Michele Volpi from the Swiss Data
920 Science Center (SDSC) is acknowledged for helpful discussions about machine learning modeling. Andrea
921 Baccarini from EPFL is acknowledged for helping produce the map in Figure 1. David Beddows from
922 University of Birmingham is acknowledged for help with the trajectory analysis.

923 **Author Contributions**

924 J.B.P. - Conceptualization, Methodology, Software, Validation, Formal Analysis, Investigation, Resources,
925 Data Curation, Writing – original draft preparation, Writing – review and editing, Visualization,
926 Supervision, Project administration.

927 J.L.H. - Conceptualization, Methodology, Software, Validation, Formal Analysis, Investigation, Resources,
928 Data Curation, Writing – original draft preparation, Writing – review and editing, Visualization,
929 Supervision, Project administration.

930 L.L.S. – Funding acquisition, Resources, Data curation, Writing – review and editing.

931 H.S. – Conceptualization, Methodology, Validation, Formal Analysis, Investigation, Resources, Data
932 Curation, Writing – original draft preparation, Funding acquisition, Writing – review and editing,
933 Supervision, Project administration.

934 **Conflicts of interest**

935 The authors declare they have no conflicts of interest.

936 **Data/code availability**

937 The data used in this study are available at [[10.5281/zenodo.11669155](https://doi.org/10.5281/zenodo.11669155)]. The original data sources are
938 (<https://ebas.nilu.no/>) for ozone, DMI (<https://www.dmi.dk/publikationer>) for meteorological data, and



939 ERDA (<https://erda.au.dk/>) for meteorological data. All code used in this study is available upon request
940 from the corresponding authors.

941

942

943



944 References

- 945 Abbatt, J. P. D., Thomas, J. L., Abrahamsson, K., Boxe, C., Granfors, A., Jones, A. E., King, M.
946 D., Saiz-Lopez, A., Shepson, P. B., Sodeau, J., Toohey, D. W., Toubin, C., von Glasow,
947 R., Wren, S. N., and Yang, X.: Halogen activation via interactions with environmental ice
948 and snow in the polar lower troposphere and other regions, *Atmos. Chem. Phys.*, 12,
949 6237–6271, <https://doi.org/10.5194/acp-12-6237-2012>, 2012.
- 950 AMAP: AMAP Assessment 2015: Black carbon and ozone as Arctic climate forcers., Arctic
951 Monitoring and Assessment Programme (AMAP), 116, 2015.
- 952 Barrie, L. A., Bottenheim, J. W., Schnell, R. C., Crutzen, P. J., and Rasmussen, R. A.: Ozone
953 destruction and photochemical reactions at polar sunrise in the lower Arctic atmosphere,
954 *Nature*, 334, 138–141, <https://doi.org/10.1038/334138a0>, 1988.
- 955 Barten, J. G. M., Ganzeveld, L. N., Steeneveld, G.-J., and Krol, M. C.: Role of oceanic ozone
956 deposition in explaining temporal variability in surface ozone at High Arctic sites,
957 *Atmospheric Chemistry and Physics*, 21, 10229–10248, <https://doi.org/10.5194/acp-21-10229-2021>, 2021.
- 959 Benavent, N., Mahajan, A. S., Li, Q., Cuevas, C. A., Schmale, J., Angot, H., Jokinen, T., Quéléver,
960 L. L. J., Blechschmidt, A.-M., Zilker, B., Richter, A., Serna, J. A., Garcia-Nieto, D.,
961 Fernandez, R. P., Skov, H., Dumitrascu, A., Simões Pereira, P., Abrahamsson, K., Bucci,
962 S., Duetsch, M., Stohl, A., Beck, I., Laurila, T., Blomquist, B., Howard, D., Archer, S. D.,
963 Bariteau, L., Helmig, D., Hueber, J., Jacobi, H.-W., Posman, K., Dada, L., Daellenbach,
964 K. R., and Saiz-Lopez, A.: Substantial contribution of iodine to Arctic ozone destruction,
965 *Nat. Geosci.*, 15, 770–773, <https://doi.org/10.1038/s41561-022-01018-w>, 2022.
- 966 Bintanja, R. and Selten, F. M.: Future increases in Arctic precipitation linked to local evaporation
967 and sea-ice retreat, *Nature*, 509, 479–482, <https://doi.org/10.1038/nature13259>, 2014.
- 968 Blechschmidt, A.-M., Richter, A., Burrows, J. P., Kaleschke, L., Strong, K., Theys, N., Weber, M.,
969 Zhao, X., and Zien, A.: An exemplary case of a bromine explosion event linked to cyclone
970 development in the Arctic, *Atmospheric Chemistry and Physics*, 16, 1773–1788,
971 <https://doi.org/10.5194/acp-16-1773-2016>, 2016.
- 972 Boccolari, M. and Parmiggiani, F.: Trends and variability of cloud fraction cover in the Arctic,
973 1982–2009, *Theor Appl Climatol*, 132, 739–749, <https://doi.org/10.1007/s00704-017-2125-6>, 2018.
- 975 Bognar, K., Zhao, X., Strong, K., Chang, R. Y.-W., Frieß, U., Hayes, P. L., McClure-Begley, A.,
976 Morris, S., Tremblay, S., and Vicente-Luis, A.: Measurements of Tropospheric Bromine
977 Monoxide Over Four Halogen Activation Seasons in the Canadian High Arctic, *Journal of
978 Geophysical Research: Atmospheres*, 125, e2020JD033015,
979 <https://doi.org/10.1029/2020jd033015>, 2020.
- 980 Boisvert, L. N., Wu, D. L., and Shie, C.-L.: Increasing evaporation amounts seen in the Arctic
981 between 2003 and 2013 from AIRS data, *Journal of Geophysical Research: Atmospheres*,
982 120, 6865–6881, <https://doi.org/10.1002/2015JD023258>, 2015.



- 983 Bottenheim, J. W. and Chan, E.: A trajectory study into the origin of spring time Arctic boundary
984 layer ozone depletion, *Journal of Geophysical Research: Atmospheres*, 111,
985 <https://doi.org/10.1029/2006JD007055>, 2006.
- 986 Bottenheim, J. W., Natcheva, S., Morin, S., and Nghiem, S. V.: Ozone in the boundary layer air
987 over the Arctic Ocean: measurements during the TARA transpolar drift 2006–2008,
988 *Atmospheric Chemistry and Physics*, 9, 4545–4557, [https://doi.org/10.5194/acp-9-4545-](https://doi.org/10.5194/acp-9-4545-2009)
989 2009, 2009.
- 990 Bougoudis, I., Blechschmidt, A.-M., Richter, A., Seo, S., Burrows, J. P., Theys, N., and Rinke, A.:
991 Long-term time series of Arctic tropospheric BrO derived from UV–VIS satellite remote
992 sensing and its relation to first-year sea ice, *Atmospheric Chemistry and Physics*, 20,
993 11869–11892, <https://doi.org/10.5194/acp-20-11869-2020>, 2020.
- 994 Brockway, N., Peterson, P. K., Bigge, K., Hajny, K. D., Shepson, P. B., Pratt, K. A., Fuentes, J.
995 D., Starn, T., Kaeser, R., Stirm, B. H., and Simpson, W. R.: Tropospheric bromine
996 monoxide vertical profiles retrieved across the Alaskan Arctic in springtime, *Atmospheric
997 Chemistry and Physics*, 24, 23–40, <https://doi.org/10.5194/acp-24-23-2024>, 2024.
- 998 Burd, J. A., Peterson, P. K., Nghiem, S. V., Perovich, D. K., and Simpson, W. R.: Snowmelt onset
999 hinders bromine monoxide heterogeneous recycling in the Arctic, *Journal of Geophysical
1000 Research: Atmospheres*, 122, 8297–8309, <https://doi.org/10.1002/2017jd026906>, 2017.
- 1001 Chen, D., Luo, Y., Yang, X., Si, F., Dou, K., Zhou, H., Qian, Y., Hu, C., Liu, J., and Liu, W.: Study
1002 of an Arctic blowing snow-induced bromine explosion event in Ny-Ålesund, Svalbard,
1003 *Science of The Total Environment*, 839, 156335,
1004 <https://doi.org/10.1016/j.scitotenv.2022.156335>, 2022.
- 1005 Christiansen, A., Mickley, L. J., Liu, J., Oman, L. D., and Hu, L.: Multidecadal increases in global
1006 tropospheric ozone derived from ozonesonde and surface site observations: can models
1007 reproduce ozone trends?, *Atmospheric Chemistry and Physics*, 22, 14751–14782,
1008 <https://doi.org/10.5194/acp-22-14751-2022>, 2022.
- 1009 Christiansen, B., Jepsen, N., Kivi, R., Hansen, G., Larsen, N., and Korsholm, U. S.: Trends and
1010 annual cycles in soundings of Arctic tropospheric ozone, *Atmospheric Chemistry and
1011 Physics*, 17, 9347–9364, <https://doi.org/10.5194/acp-17-9347-2017>, 2017.
- 1012 Collaud Coen, M., Andrews, E., Alastuey, A., Arsov, T. P., Backman, J., Brem, B. T., Bukowiecki,
1013 N., Couret, C., Eleftheriadis, K., Flentje, H., Fiebig, M., Gysel-Beer, M., Hand, J. L., Hoffer,
1014 A., Hooda, R., Hueglin, C., Joubert, W., Keywood, M., Kim, J. E., Kim, S. W.,
1015 Labuschagne, C., Lin, N. H., Lin, Y., Lund Myhre, C., Luoma, K., Lyamani, H., Marinoni,
1016 A., Mayol-Bracero, O. L., Mihalopoulos, N., Pandolfi, M., Prats, N., Prenni, A. J., Putaud,
1017 J. P., Ries, L., Reisen, F., Sellegri, K., Sharma, S., Sheridan, P., Sherman, J. P., Sun, J.,
1018 Titos, G., Torres, E., Tuch, T., Weller, R., Wiedensohler, A., Zieger, P., and Laj, P.:
1019 Multidecadal trend analysis of in situ aerosol radiative properties around the world, *Atmos.
1020 Chem. Phys.*, 20, 8867–8908, <https://doi.org/10.5194/acp-20-8867-2020>, 2020.
- 1021 Confer, K. L., Jaeglé, L., Liston, G. E., Sharma, S., Nandan, V., Yackel, J., Ewert, M., and
1022 Horowitz, H. M.: Impact of Changing Arctic Sea Ice Extent, Sea Ice Age, and Snow Depth
1023 on Sea Salt Aerosol From Blowing Snow and the Open Ocean for 1980–2017, *Journal of*



- 1024 Geophysical Research: Atmospheres, 128, e2022JD037667,
1025 <https://doi.org/10.1029/2022JD037667>, 2023.
- 1026 Cooper, O. R., Schultz, M. G., Schröder, S., Chang, K.-L., Gaudel, A., Benítez, G. C., Cuevas,
1027 E., Fröhlich, M., Galbally, I. E., Molloy, S., Kubistin, D., Lu, X., McClure-Begley, A.,
1028 Nédélec, P., O'Brien, J., Oltmans, S. J., Petropavlovskikh, I., Ries, L., Senik, I., Sjöberg,
1029 K., Solberg, S., Spain, G. T., Spangl, W., Steinbacher, M., Tarasick, D., Thouret, V., and
1030 Xu, X.: Multi-decadal surface ozone trends at globally distributed remote locations,
1031 *Elementa: Science of the Anthropocene*, 8, 23, <https://doi.org/10.1525/elementa.420>,
1032 2020.
- 1033 Draxler, R. R. and Hess, G. D.: An overview of the HYSPLIT_4 modelling system for trajectories,
1034 dispersion and deposition, *Australian Meteorological Magazine*, 47, 295–308, 1998.
- 1035 Eneroth, K., Holmén, K., Berg, T., Schmidbauer, N., and Solberg, S.: Springtime depletion of
1036 tropospheric ozone, gaseous elemental mercury and non-methane hydrocarbons in the
1037 European Arctic, and its relation to atmospheric transport, *Atmospheric Environment*, 41,
1038 8511–8526, <https://doi.org/10.1016/j.atmosenv.2007.07.008>, 2007.
- 1039 Flyger, H., Heidam, N. Z., Hansen, K. A., Rasmussen, L., and Megaw, W. J.: The background
1040 levels of the summer tropospheric aerosol and trace gases in Greenland, *Journal of*
1041 *Aerosol Science*, 11, 95–110, [https://doi.org/10.1016/0021-8502\(80\)90149-4](https://doi.org/10.1016/0021-8502(80)90149-4), 1980.
- 1042 Frieß, U., Hollwedel, J., König-Langlo, G., Wagner, T., and Platt, U.: Dynamics and chemistry of
1043 tropospheric bromine explosion events in the Antarctic coastal region, *Journal of*
1044 *Geophysical Research: Atmospheres*, 109, <https://doi.org/10.1029/2003JD004133>, 2004.
- 1045 Gao, Z., Geilfus, N.-X., Saiz-Lopez, A., and Wang, F.: Reproducing Arctic springtime tropospheric
1046 ozone and mercury depletion events in an outdoor mesocosm sea ice facility, *Atmos.*
1047 *Chem. Phys.*, 22, 1811–1824, <https://doi.org/10.5194/acp-22-1811-2022>, 2022.
- 1048 Gryning, S.-E., Batchvarova, E., Floors, R., Münkel, C., Sørensen, L. L., and Skov, H.: Observed
1049 aerosol-layer depth at Station Nord in the high Arctic, *International Journal of Climatology*,
1050 43, 3247–3263, <https://doi.org/10.1002/joc.8027>, 2023.
- 1051 Halfacre, J. W., Knepp, T. N., Shepson, P. B., Thompson, C. R., Pratt, K. A., Li, B., Peterson, P.
1052 K., Walsh, S. J., Simpson, W. R., Matrai, P. A., Bottenheim, J. W., Natcheva, S., Perovich,
1053 D. K., and Richter, A.: Temporal and spatial characteristics of ozone depletion events from
1054 measurements in the Arctic, *Atmos. Chem. Phys.*, 14, 4875–4894,
1055 <https://doi.org/10.5194/acp-14-4875-2014>, 2014.
- 1056 Halfacre, J. W., Shepson, P. B., and Pratt, K. A.: pH-dependent production of molecular chlorine,
1057 bromine, and iodine from frozen saline surfaces, *Atmos. Chem. Phys.*, 19, 4917–4931,
1058 <https://doi.org/10.5194/acp-19-4917-2019>, 2019.
- 1059 Heidam, N. Z., Whlin, P., and Christensen, J. H.: Tropospheric Gases and Aerosols in Northeast
1060 Greenland, *Journal of the Atmospheric Sciences*, 56, 261–278,
1061 [https://doi.org/10.1175/1520-0469\(1999\)056<0261:Tgaain>2.0.Co;2](https://doi.org/10.1175/1520-0469(1999)056<0261:Tgaain>2.0.Co;2), 1999.



- 1062 Heidam, N. Z., Christensen, J., Wahlin, P., and Skov, H.: Arctic atmospheric contaminants in NE
1063 Greenland: levels, variations, origins, transport, transformations and trends 1990–2001,
1064 *Sci Total Environ*, 331, 5–28, <https://doi.org/10.1016/j.scitotenv.2004.03.033>, 2004.
- 1065 Helmig, D., Oltmans, S. J., Carlson, D., Lamarque, J.-F., Jones, A., Labuschagne, C., Anlauf, K.,
1066 and Hayden, K.: A review of surface ozone in the polar regions, *Atmospheric Environment*,
1067 41, 5138–5161, <https://doi.org/10.1016/j.atmosenv.2006.09.053>, 2007a.
- 1068 Helmig, D., Oltmans, S. J., Morse, T. O., and Dibb, J. E.: What is causing high ozone at Summit,
1069 Greenland?, *Atmospheric Environment*, 41, 5031–5043,
1070 <https://doi.org/10.1016/j.atmosenv.2006.05.084>, 2007b.
- 1071 Helmig, D., Boylan, P., Johnson, B., Oltmans, S., Fairall, C., Staebler, R., Weinheimer, A.,
1072 Orlando, J., Knapp, D. J., Montzka, D. D., Flocke, F., Frieß, U., Sihler, H., and Shepson,
1073 P. B.: Ozone dynamics and snow-atmosphere exchanges during ozone depletion events
1074 at Barrow, Alaska, *Journal of Geophysical Research: Atmospheres*, 117,
1075 <https://doi.org/10.1029/2012JD017531>, 2012.
- 1076 Herrmann, M., Schöne, M., Borger, C., Warnach, S., Wagner, T., Platt, U., and Gutheil, E.: Ozone
1077 depletion events in the Arctic spring of 2019: a new modeling approach to bromine
1078 emissions, *Atmospheric Chemistry and Physics*, 22, 13495–13526,
1079 <https://doi.org/10.5194/acp-22-13495-2022>, 2022.
- 1080 Hersbach, H., Bell, B., Berrisford, P., Hirahara, S., Horányi, A., Muñoz-Sabater, J., Nicolas, J.,
1081 Peubey, C., Radu, R., Schepers, D., Simmons, A., Soci, C., Abdalla, S., Abellan, X.,
1082 Balsamo, G., Bechtold, P., Biavati, G., Bidlot, J., Bonavita, M., Chiara, G., Dahlgren, P.,
1083 Dee, D., Diamantakis, M., Dragani, R., Flemming, J., Forbes, R., Fuentes, M., Geer, A.,
1084 Haimberger, L., Healy, S., Hogan, R. J., Hólm, E., Janisková, M., Keeley, S., Laloyaux,
1085 P., Lopez, P., Lupu, C., Radnoti, G., Rosnay, P., Rozum, I., Vamborg, F., Villaume, S.,
1086 and Thépaut, J.: The ERA5 global reanalysis, *Quarterly Journal of the Royal
1087 Meteorological Society*, 146, 1999–2049, <https://doi.org/10.1002/qj.3803>, 2020.
- 1088 Heslin-Rees, D., Burgos, M., Hansson, H. C., Krejci, R., Ström, J., Tunved, P., and Zieger, P.:
1089 From a polar to a marine environment: has the changing Arctic led to a shift in aerosol
1090 light scattering properties?, *Atmos. Chem. Phys.*, 20, 13671–13686,
1091 <https://doi.org/10.5194/acp-20-13671-2020>, 2020.
- 1092 Hirdman, D., Sodemann, H., Eckhardt, S., Burkhart, J. F., Jefferson, A., Mefford, T., Quinn, P. K.,
1093 Sharma, S., Ström, J., and Stohl, A.: Source identification of short-lived air pollutants in
1094 the Arctic using statistical analysis of measurement data and particle dispersion model
1095 output, *Atmos. Chem. Phys.*, 10, 669–693, <https://doi.org/10.5194/acp-10-669-2010>,
1096 2010.
- 1097 Hogan, R.: *Radiation Quantities in the ECMWF model and MARS*, 2015.
- 1098 Hopper, J. F., Barrie, L. A., Silis, A., Hart, W., Gallant, A. J., and Dryfhout, H.: Ozone and
1099 meteorology during the 1994 Polar Sunrise Experiment, *Journal of Geophysical Research:
1100 Atmospheres*, 103, 1481–1492, <https://doi.org/10.1029/97JD02888>, 1998.
- 1101 Ianniello, A., Salzano, R., Salvatori, R., Esposito, G., Spataro, F., Montagnoli, M., Mabilia, R., and
1102 Pasini, A.: Nitrogen Oxides (NO_x) in the Arctic Troposphere at Ny-Ålesund (Svalbard



- 1103 Islands): Effects of Anthropogenic Pollution Sources, *Atmosphere*, 12, 901,
1104 <https://doi.org/10.3390/atmos12070901>, 2021.
- 1105 Jacobi, H.-W., Morin, S., and Bottenheim, J. W.: Observation of widespread depletion of ozone in
1106 the springtime boundary layer of the central Arctic linked to mesoscale synoptic conditions,
1107 *Journal of Geophysical Research: Atmospheres*, 115,
1108 <https://doi.org/10.1029/2010JD013940>, 2010.
- 1109 Jenkins, M. T. and Dai, A.: Arctic Climate Feedbacks in ERA5 Reanalysis: Seasonal and Spatial
1110 Variations and the Impact of Sea-Ice Loss, *Geophysical Research Letters*, 49,
1111 e2022GL099263, <https://doi.org/10.1029/2022GL099263>, 2022.
- 1112 Jensen, C. D.: Weather Observations from Greenland 1958-2022, Danish Meteorological
1113 Institute, 2022.
- 1114 Jeong, D., McNamara, S. M., Barget, A. J., Raso, A. R. W., Upchurch, L. M., Thanekar, S., Quinn,
1115 P. K., Simpson, W. R., Fuentes, J. D., Shepson, P. B., and Pratt, K. A.: Multiphase
1116 Reactive Bromine Chemistry during Late Spring in the Arctic: Measurements of Gases,
1117 Particles, and Snow, *ACS Earth Space Chem.*, 6, 2877–2887,
1118 <https://doi.org/10.1021/acsearthspacechem.2c00189>, 2022.
- 1119 Jones, A. E., Anderson, P. S., Begoin, M., Brough, N., Hutterli, M. A., Marshall, G. J., Richter, A.,
1120 Roscoe, H. K., and Wolff, E. W.: BrO, blizzards, and drivers of polar tropospheric ozone
1121 depletion events, *Atmospheric Chemistry and Physics*, 9, 4639–4652,
1122 <https://doi.org/10.5194/acp-9-4639-2009>, 2009.
- 1123 Kaleschke, L., Richter, A., Burrows, J., Afe, O., Heygster, G., Notholt, J., Rankin, A. M., Roscoe,
1124 H. K., Hollwedel, J., Wagner, T., and Jacobi, H. W.: Frost flowers on sea ice as a source
1125 of sea salt and their influence on tropospheric halogen chemistry, *Geophysical Research
1126 Letters*, 31, <https://doi.org/10.1029/2004gl020655>, 2004.
- 1127 Kalnay, E., Kanamitsu, M., Kistler, R., Collins, W., Deaven, D., Gandin, L., Iredell, M., Saha, S.,
1128 White, G., Woollen, J., Zhu, Y., Chelliah, M., Ebisuzaki, W., Higgins, W., Janowiak, J., Mo,
1129 K. C., Ropelewski, C., Wang, J., Leetmaa, A., Reynolds, R., Jenne, R., and Joseph, D.:
1130 The NCEP/NCAR 40-Year Reanalysis Project, *Bulletin of the American Meteorological
1131 Society*, 77, 437–472, [https://doi.org/10.1175/1520-
1132 0477\(1996\)077<0437:TNYRP>2.0.CO;2](https://doi.org/10.1175/1520-0477(1996)077<0437:TNYRP>2.0.CO;2), 1996.
- 1133 Kendall, M. G.: Rank correlation methods, Griffin, Oxford, England, 1948.
- 1134 Kim, Y.-H., Min, S.-K., Gillett, N. P., Notz, D., and Malinina, E.: Observationally-constrained
1135 projections of an ice-free Arctic even under a low emission scenario, *Nat Commun*, 14,
1136 3139, <https://doi.org/10.1038/s41467-023-38511-8>, 2023.
- 1137 Koo, J. H., Wang, Y., Kurosu, T. P., Chance, K., Rozanov, A., Richter, A., Oltmans, S. J.,
1138 Thompson, A. M., Hair, J. W., Fenn, M. A., Weinheimer, A. J., Ryerson, T. B., Solberg, S.,
1139 Huey, L. G., Liao, J., Dibb, J. E., Neuman, J. A., Nowak, J. B., Pierce, R. B., Natarajan,
1140 M., and Al-Saadi, J.: Characteristics of tropospheric ozone depletion events in the Arctic
1141 spring: analysis of the ARCTAS, ARCPAC, and ARCIONS measurements and satellite
1142 BrO observations, *Atmos. Chem. Phys.*, 12, 9909–9922, [https://doi.org/10.5194/acp-12-
1143 9909-2012](https://doi.org/10.5194/acp-12-9909-2012), 2012.



- 1144 Kwok, R.: Arctic sea ice thickness, volume, and multiyear ice coverage: losses and coupled
1145 variability (1958–2018), *Environ. Res. Lett.*, 13, 105005, <https://doi.org/10.1088/1748-9326/aae3ec>, 2018.
- 1147 Lacis, A. A., Wuebbles, D. J., and Logan, J. A.: Radiative forcing of climate by changes in the
1148 vertical distribution of ozone, *Journal of Geophysical Research: Atmospheres*, 95, 9971–
1149 9981, <https://doi.org/10.1029/JD095iD07p09971>, 1990.
- 1150 Law, K. S., Hjorth, J. L., Pernov, J. B., Whaley, C. H., Skov, H., Collaud Coen, M., Langner, J.,
1151 Arnold, S. R., Tarasick, D., Christensen, J., Deushi, M., Effertz, P., Faluvegi, G., Gauss,
1152 M., Im, U., Oshima, N., Petropavlovskikh, I., Plummer, D., Tsigaridis, K., Tsyro, S.,
1153 Solberg, S., and Turnock, S.: Arctic Tropospheric Ozone Trends, *Geophysical Research
1154 Letters*, 50, e2023GL103096, <https://doi.org/10.1029/2023GL103096>, 2023.
- 1155 Lelli, L., Vountas, M., Khosravi, N., and Burrows, J. P.: Satellite remote sensing of regional and
1156 seasonal Arctic cooling showing a multi-decadal trend towards brighter and more liquid
1157 clouds, *Atmospheric Chemistry and Physics*, 23, 2579–2611, <https://doi.org/10.5194/acp-23-2579-2023>, 2023.
- 1159 Mann, H. B.: Nonparametric Tests Against Trend, *Econometrica*, 13, 245–259,
1160 <https://doi.org/10.2307/1907187>, 1945.
- 1161 Marelle, L., Thomas, J. L., Ahmed, S., Tuite, K., Stutz, J., Dommergue, A., Simpson, W. R., Frey,
1162 M. M., and Baladima, F.: Implementation and Impacts of Surface and Blowing Snow
1163 Sources of Arctic Bromine Activation Within WRF-Chem 4.1.1, *Journal of Advances in
1164 Modeling Earth Systems*, 13, e2020MS002391, <https://doi.org/10.1029/2020MS002391>,
1165 2021.
- 1166 McNamara, S. M., Garner, N. M., Wang, S., Raso, A. R. W., Thanekar, S., Barget, A. J., Fuentes,
1167 J. D., Shepson, P. B., and Pratt, K. A.: Bromine Chloride in the Coastal Arctic: Diel Patterns
1168 and Production Mechanisms, *ACS Earth and Space Chemistry*,
1169 <https://doi.org/10.1021/acsearthspacechem.0c00021>, 2020.
- 1170 Monks, P. S., Archibald, A. T., Colette, A., Cooper, O., Coyle, M., Derwent, R., Fowler, D., Granier,
1171 C., Law, K. S., Mills, G. E., Stevenson, D. S., Tarasova, O., Thouret, V., von
1172 Schneidmesser, E., Sommariva, R., Wild, O., and Williams, M. L.: Tropospheric ozone
1173 and its precursors from the urban to the global scale from air quality to short-lived climate
1174 forcer, *Atmos. Chem. Phys.*, 15, 8889–8973, <https://doi.org/10.5194/acp-15-8889-2015>,
1175 2015.
- 1176 Moore, C. W., Obrist, D., Steffen, A., Staebler, R. M., Douglas, T. A., Richter, A., and Nghiem, S.
1177 V.: Convective forcing of mercury and ozone in the Arctic boundary layer induced by leads
1178 in sea ice, *Nature*, 506, 81–4, <https://doi.org/10.1038/nature12924>, 2014.
- 1179 Morin, S., Savarino, J., Frey, M. M., Yan, N., Bekki, S., Bottenheim, J. W., and Martins, J. M. F.:
1180 Tracing the Origin and Fate of NO_x in the Arctic Atmosphere Using Stable Isotopes in
1181 Nitrate, *Science*, 322, 730–732, <https://doi.org/10.1126/science.1161910>, 2008.
- 1182 Neuman, J. A., Nowak, J. B., Huey, L. G., Burkholder, J. B., Dibb, J. E., Holloway, J. S., Liao, J.,
1183 Peischl, J., Roberts, J. M., Ryerson, T. B., Scheuer, E., Stark, H., Stickel, R. E., Tanner,
1184 D. J., and Weinheimer, A.: Bromine measurements in ozone depleted air over the Arctic



- 1185 Ocean, Atmospheric Chemistry and Physics, 10, 6503–6514, [https://doi.org/10.5194/acp-](https://doi.org/10.5194/acp-10-6503-2010)
1186 10-6503-2010, 2010.
- 1187 Nguyen, Q. T., Skov, H., Sorensen, L. L., Jensen, B. J., Grube, A. G., Massling, A., Glasius, M.,
1188 and Nojgaard, J. K.: Source apportionment of particles at Station Nord, North East
1189 Greenland during 2008–2010 using COPREM and PMF analysis, *Atmos. Chem. Phys.*,
1190 13, 35–49, <https://doi.org/10.5194/acp-13-35-2013>, 2013.
- 1191 Nguyen, Q. T., Glasius, M., Sorensen, L. L., Jensen, B., Skov, H., Birmili, W., Wiedensohler, A.,
1192 Kristensson, A., Nojgaard, J. K., and Massling, A.: Seasonal variation of atmospheric
1193 particle number concentrations, new particle formation and atmospheric oxidation
1194 capacity at the high Arctic site Villum Research Station, Station Nord, *Atmos. Chem.*
1195 *Phys.*, 16, 11319–11336, <https://doi.org/10.5194/acp-16-11319-2016>, 2016.
- 1196 Notz, D. and Community, S.: Arctic Sea Ice in CMIP6, *Geophysical Research Letters*, 47,
1197 e2019GL086749, <https://doi.org/10.1029/2019GL086749>, 2020.
- 1198 Oltmans, S. J., Johnson, B. J., and Harris, J. M.: Springtime boundary layer ozone depletion at
1199 Barrow, Alaska: Meteorological influence, year-to-year variation, and long-term change,
1200 *Journal of Geophysical Research: Atmospheres*, 117,
1201 <https://doi.org/10.1029/2011JD016889>, 2012.
- 1202 Pernov, J. B., Bossi, R., Lebourgeois, T., Nøjgaard, J. K., Holzinger, R., Hjorth, J. L., and Skov,
1203 H.: Atmospheric VOC measurements at a High Arctic site: characteristics and source
1204 apportionment, *Atmos. Chem. Phys.*, 21, 2895–2916, [https://doi.org/10.5194/acp-21-](https://doi.org/10.5194/acp-21-2895-2021)
1205 2895-2021, 2021.
- 1206 Pernov, J. B., Beddows, D., Thomas, D. C., Dall’Osto, M., Harrison, R. M., Schmale, J., Skov, H.,
1207 and Massling, A.: Increased aerosol concentrations in the High Arctic attributable to
1208 changing atmospheric transport patterns, *npj Clim Atmos Sci*, 5, 1–13,
1209 <https://doi.org/10.1038/s41612-022-00286-y>, 2022.
- 1210 Pernov, J. B., Gros-Daillon, J., and Schmale, J.: Comparison of selected surface level ERA5
1211 variables against in situ observations in the continental Arctic, *Quarterly Journal of the*
1212 *Royal Meteorological Society*, 1–24, <https://doi.org/10.1002/qj.4700>, 2024.
- 1213 Peterson, P. K., Simpson, W. R., Pratt, K. A., Shepson, P. B., Frieß, U., Zielcke, J., Platt, U.,
1214 Walsh, S. J., and Nghiem, S. V.: Dependence of the vertical distribution of bromine
1215 monoxide in the lower troposphere on meteorological factors such as wind speed and
1216 stability, *Atmos. Chem. Phys.*, 15, 2119–2137, <https://doi.org/10.5194/acp-15-2119-2015>,
1217 2015.
- 1218 Peterson, P. K., Pöhler, D., Sihler, H., Zielcke, J., General, S., Frieß, U., Platt, U., Simpson, W.
1219 R., Nghiem, S. V., Shepson, P. B., Stirm, B. H., Dhaniyala, S., Wagner, T., Caulton, D. R.,
1220 Fuentes, J. D., and Pratt, K. A.: Observations of bromine monoxide transport in the Arctic
1221 sustained on aerosol particles, *Atmos. Chem. Phys.*, 17, 7567–7579,
1222 <https://doi.org/10.5194/acp-17-7567-2017>, 2017.
- 1223 Peterson, P. K., Pöhler, D., Zielcke, J., General, S., Frieß, U., Platt, U., Simpson, W. R., Nghiem,
1224 S. V., Shepson, P. B., Stirm, B. H., and Pratt, K. A.: Springtime Bromine Activation over



- 1225 Coastal and Inland Arctic Snowpacks, *ACS Earth and Space Chemistry*, 2, 1075–1086,
1226 <https://doi.org/10.1021/acsearthspacechem.8b00083>, 2018.
- 1227 Peterson, P. K., Hartwig, M., May, N. W., Schwartz, E., Rigor, I., Ermold, W., Steele, M., Morison,
1228 J. H., Nghiem, S. V., and Pratt, K. A.: Snowpack measurements suggest role for multi-
1229 year sea ice regions in Arctic atmospheric bromine and chlorine chemistry, *Elementa:
1230 Science of the Anthropocene*, 7, <https://doi.org/10.1525/elementa.352>, 2019.
- 1231 Pöhler, D., Vogel, L., Frieß, U., and Platt, U.: Observation of halogen species in the Amundsen
1232 Gulf, Arctic, by active long-path differential optical absorption spectroscopy, *Proceedings
1233 of the National Academy of Sciences*, 107, 6582–6587,
1234 <https://doi.org/10.1073/pnas.0912231107>, 2010.
- 1235 Pratt, K. A., Custard, K. D., Shepson, P. B., Douglas, T. A., Pöhler, D., General, S., Zielcke, J.,
1236 Simpson, W. R., Platt, U., Tanner, D. J., Gregory Huey, L., Carlsen, M., and Stirn, B. H.:
1237 Photochemical production of molecular bromine in Arctic surface snowpacks, *Nature
1238 Geoscience*, 6, 351–356, <https://doi.org/10.1038/ngeo1779>, 2013.
- 1239 Rantanen, M., Karpechko, A. Yu., Lipponen, A., Nordling, K., Hyvärinen, O., Ruosteenoja, K.,
1240 Vihma, T., and Laaksonen, A.: The Arctic has warmed nearly four times faster than the
1241 globe since 1979, *Communications Earth & Environment*, 3, 168,
1242 <https://doi.org/10.1038/s43247-022-00498-3>, 2022.
- 1243 Raso, A. R. W., Custard, K. D., May, N. W., Tanner, D., Newburn, M. K., Walker, L., Moore, R.
1244 J., Huey, L. G., Alexander, L., Shepson, P. B., and Pratt, K. A.: Active molecular iodine
1245 photochemistry in the Arctic, *Proc Natl Acad Sci U S A*, 114, 10053–10058,
1246 <https://doi.org/10.1073/pnas.1702803114>, 2017.
- 1247 Rolph, G., Stein, A., and Stunder, B.: Real-time Environmental Applications and Display sYstem:
1248 READY, *Environmental Modelling & Software*, 95, 210–228,
1249 <https://doi.org/10.1016/j.envsoft.2017.06.025>, 2017.
- 1250 Schroeder, W. H., Anlauf, K. G., Barrie, L. A., Lu, J. Y., Steffen, A., Schneeberger, D. R., and
1251 Berg, T.: Arctic springtime depletion of mercury, *Nature*, 394, 331–332,
1252 <https://doi.org/10.1038/28530>, 1998.
- 1253 Seabrook, J. and Whiteway, J.: Influence of mountains on Arctic tropospheric ozone, *Journal of
1254 Geophysical Research: Atmospheres*, 121, 1935–1942,
1255 <https://doi.org/10.1002/2015JD024114>, 2016.
- 1256 Seinfeld, J. H. and Pandis, S. N.: *Atmospheric Chemistry and Physics: From Air Pollution to
1257 Climate Change*, 3rd ed., John Wiley & Sons, 1152 pp., 2016.
- 1258 Sen, P. K.: Estimates of the Regression Coefficient Based on Kendall's Tau, *Journal of the
1259 American Statistical Association*, 63, 1379–1389,
1260 <https://doi.org/10.1080/01621459.1968.10480934>, 1968.
- 1261 Seo, S., Richter, A., Blechschmidt, A.-M., Bougoudis, I., and Burrows, J. P.: Spatial distribution of
1262 enhanced BrO and its relation to meteorological parameters in Arctic and Antarctic sea
1263 ice regions, *Atmospheric Chemistry and Physics*, 20, 12285–12312,
1264 <https://doi.org/10.5194/acp-20-12285-2020>, 2020.



- 1265 Simpson, W. R., Alvarez-Aviles, L., Douglas, T. A., Sturm, M., and Domine, F.: Halogens in the
1266 coastal snow pack near Barrow, Alaska: Evidence for active bromine air-snow chemistry
1267 during springtime, *Geophysical Research Letters*, 32,
1268 <https://doi.org/10.1029/2004GL021748>, 2005.
- 1269 Simpson, W. R., Carlson, D., Hönninger, G., Douglas, T. A., Sturm, M., Perovich, D., and Platt,
1270 U.: First-year sea-ice contact predicts bromine monoxide (BrO) levels at Barrow, Alaska
1271 better than potential frost flower contact, *Atmospheric Chemistry and Physics*, 7, 621–627,
1272 <https://doi.org/10.5194/acp-7-621-2007>, 2007a.
- 1273 Simpson, W. R., von Glasow, R., Riedel, K., Anderson, P., Ariya, P., Bottenheim, J., Burrows, J.,
1274 Carpenter, L. J., Frieß, U., Goodsite, M. E., Heard, D., Hutterli, M., Jacobi, H. W.,
1275 Kaleschke, L., Neff, B., Plane, J., Platt, U., Richter, A., Roscoe, H., Sander, R., Shepson,
1276 P., Sodeau, J., Steffen, A., Wagner, T., and Wolff, E.: Halogens and their role in polar
1277 boundary-layer ozone depletion, *Atmos. Chem. Phys.*, 7, 4375–4418,
1278 <https://doi.org/10.5194/acp-7-4375-2007>, 2007b.
- 1279 Simpson, W. R., Brown, S. S., Saiz-Lopez, A., Thornton, J. A., and Glasow, R.: Tropospheric
1280 halogen chemistry: sources, cycling, and impacts, *Chem Rev*, 115, 4035–62,
1281 <https://doi.org/10.1021/cr5006638>, 2015.
- 1282 Skov, H., Christensen, J. H., Goodsite, M. E., Heidam, N. Z., Jensen, B., Wahlin, P., and
1283 Geernaert, G.: Fate of elemental mercury in the arctic during atmospheric mercury
1284 depletion episodes and the load of atmospheric mercury to the arctic, *Environ. Sci.
1285 Technol.*, 38, 2373–2382, <https://doi.org/10.1021/es030080h>, 2004.
- 1286 Skov, H., Hjorth, J., Nordstrøm, C., Jensen, B., Christoffersen, C., Bech Poulsen, M., Baldtzer
1287 Liisberg, J., Beddows, D., Dall'Osto, M., and Christensen, J. H.: Variability in gaseous
1288 elemental mercury at Villum Research Station, Station Nord, in North Greenland from
1289 1999 to 2017, *Atmos. Chem. Phys.*, 20, 13253–13265, <https://doi.org/10.5194/acp-20-13253-2020>, 2020.
- 1291 Solberg, S., Schmidbauer, N., Semb, A., Stordal, F., and Hov, Ø.: Boundary-layer ozone depletion
1292 as seen in the Norwegian Arctic in spring, *Journal of Atmospheric Chemistry*, 23, 301–
1293 332, <https://doi.org/10.1007/BF00055158>, 1996.
- 1294 Stein, A. F., Draxler, R. R., Rolph, G. D., Stunder, B. J. B., Cohen, M. D., and Ngan, F.: NOAA's
1295 HYSPLIT Atmospheric Transport and Dispersion Modeling System, *Bulletin of the
1296 American Meteorological Society*, 96, 2059–2077, <https://doi.org/10.1175/bams-d-14-00110.1>, 2015.
- 1298 Stevenson, D. S., Young, P. J., Naik, V., Lamarque, J.-F., Shindell, D. T., Voulgarakis, A., Skeie,
1299 R. B., Dalsoren, S. B., Myhre, G., Berntsen, T. K., Folberth, G. A., Rumbold, S. T., Collins,
1300 W. J., MacKenzie, I. A., Doherty, R. M., Zeng, G., van Noije, T. P. C., Strunk, A.,
1301 Bergmann, D., Cameron-Smith, P., Plummer, D. A., Strode, S. A., Horowitz, L., Lee, Y.
1302 H., Szopa, S., Sudo, K., Nagashima, T., Josse, B., Cionni, I., Righi, M., Eyring, V., Conley,
1303 A., Bowman, K. W., Wild, O., and Archibald, A.: Tropospheric ozone changes, radiative
1304 forcing and attribution to emissions in the Atmospheric Chemistry and Climate Model
1305 Intercomparison Project (ACCMIP), *Atmos. Chem. Phys.*, 13, 3063–3085,
1306 <https://doi.org/10.5194/acp-13-3063-2013>, 2013.



- 1307 Stohl, A.: Computation, accuracy and applications of trajectories - A review and bibliography,
1308 Atmospheric Environment, 32, 947–966, [https://doi.org/10.1016/s1352-2310\(97\)00457-3](https://doi.org/10.1016/s1352-2310(97)00457-3),
1309 1998.
- 1310 Stohl, A.: Characteristics of atmospheric transport into the Arctic troposphere, Journal of
1311 Geophysical Research, 111, <https://doi.org/10.1029/2005jd006888>, 2006.
- 1312 Stroeve, J. and Notz, D.: Changing state of Arctic sea ice across all seasons, Environ. Res. Lett.,
1313 13, 103001, <https://doi.org/10.1088/1748-9326/aade56>, 2018.
- 1314 Strong, C., Fuentes, J. D., Davis, R. E., and Bottenheim, J. W.: Thermodynamic attributes of
1315 Arctic boundary layer ozone depletion, Atmospheric Environment, 36, 2641–2652,
1316 [https://doi.org/10.1016/S1352-2310\(02\)00114-0](https://doi.org/10.1016/S1352-2310(02)00114-0), 2002.
- 1317 Sviashchennikov, P. and Drugorub, A.: Long-term trends in total cloud cover in the Arctic based
1318 on surface observations in 1985–2020, Bulletin of Geography. Physical Geography
1319 Series, 33–43, <https://doi.org/10.12775/bgeo-2022-0003>, 2022.
- 1320 Swanson, W. F., Graham, K. A., Halfacre, J. W., Holmes, C. D., Shepson, P. B., and Simpson,
1321 W. R.: Arctic Reactive Bromine Events Occur in Two Distinct Sets of Environmental
1322 Conditions: A Statistical Analysis of 6 Years of Observations, Journal of Geophysical
1323 Research: Atmospheres, 125, e2019JD032139, <https://doi.org/10.1029/2019JD032139>,
1324 2020.
- 1325 Swanson, W. F., Holmes, C. D., Simpson, W. R., Confer, K., Marelle, L., Thomas, J. L., Jaeglé,
1326 L., Alexander, B., Zhai, S., Chen, Q., Wang, X., and Sherwen, T.: Comparison of model
1327 and ground observations finds snowpack and blowing snow aerosols both contribute to
1328 Arctic tropospheric reactive bromine, Atmospheric Chemistry and Physics, 22, 14467–
1329 14488, <https://doi.org/10.5194/acp-22-14467-2022>, 2022.
- 1330 Tarasick, D. W. and Bottenheim, J. W.: Surface ozone depletion episodes in the Arctic and
1331 Antarctic from historical ozonesonde records, Atmos. Chem. Phys., 2, 197–205,
1332 <https://doi.org/10.5194/acp-2-197-2002>, 2002.
- 1333 Theil, H.: A rank-invariant method of linear and polynomial regression analysis, Nederl. Akad.
1334 Wetensch., Proc., 53, 386–392, 1950.
- 1335 Tschudi, M., Meier, W. N., Stewart, J. S., Fowler, C., and Maslanik, J.: EASE-Grid Sea Ice Age,
1336 Version 4, NASA National Snow and Ice Data Center Distributed Active Archive Center,
1337 <https://doi.org/10.5067/UTAV7490FEPB>, 2019.
- 1338 Wang, S., McNamara, S. M., Moore, C. W., Obrist, D., Steffen, A., Shepson, P. B., Staebler, R.
1339 M., Raso, A. R. W., and Pratt, K. A.: Direct detection of atmospheric atomic bromine
1340 leading to mercury and ozone depletion, Proc Natl Acad Sci U S A, 116, 14479–14484,
1341 <https://doi.org/10.1073/pnas.1900613116>, 2019.
- 1342 Wang, X., Liu, J., Yang, B., Bao, Y., Petropoulos, G. P., Liu, H., and Hu, B.: Seasonal Trends in
1343 Clouds and Radiation over the Arctic Seas from Satellite Observations during 1982 to
1344 2019, Remote Sensing, 13, 3201, <https://doi.org/10.3390/rs13163201>, 2021.



- 1345 Whaley, C. H., Law, K. S., Hjorth, J. L., Skov, H., Arnold, S. R., Langner, J., Pernov, J. B.,
1346 Bergeron, G., Bourgeois, I., Christensen, J. H., Chien, R.-Y., Deushi, M., Dong, X., Effertz,
1347 P., Faluvegi, G., Flanner, M., Fu, J. S., Gauss, M., Huey, G., Im, U., Kivi, R., Marelle, L.,
1348 Onishi, T., Oshima, N., Petropavlovskikh, I., Peischl, J., Plummer, D. A., Pozzoli, L., Raut,
1349 J.-C., Ryerson, T., Skeie, R., Solberg, S., Thomas, M. A., Thompson, C., Tsigaridis, K.,
1350 Tsyro, S., Turnock, S. T., von Salzen, K., and Tarasick, D. W.: Arctic tropospheric ozone:
1351 assessment of current knowledge and model performance, *Atmospheric Chemistry and*
1352 *Physics*, 23, 637–661, <https://doi.org/10.5194/acp-23-637-2023>, 2023.
- 1353 Yang, X., Blechschmidt, A. M., Bognar, K., McClure-Begley, A., Morris, S., Petropavlovskikh, I.,
1354 Richter, A., Skov, H., Strong, K., Tarasick, D. W., Uttal, T., Vestenius, M., and Zhao, X.:
1355 Pan-Arctic surface ozone: modelling vs. measurements, *Atmos. Chem. Phys.*, 20, 15937–
1356 15967, <https://doi.org/10.5194/acp-20-15937-2020>, 2020.
- 1357 Zeng, T., Wang, Y., Chance, K., Blake, N., Blake, D., and Ridley, B.: Halogen-driven low-altitude
1358 O₃ and hydrocarbon losses in spring at northern high latitudes, *Journal of Geophysical*
1359 *Research: Atmospheres*, 111, <https://doi.org/10.1029/2005JD006706>, 2006.
- 1360 Zhao, X., Strong, K., Adams, C., Schofield, R., Yang, X., Richter, A., Friess, U., Blechschmidt, A.-
1361 M., and Koo, J.-H.: A case study of a transported bromine explosion event in the Canadian
1362 high arctic, *Journal of Geophysical Research: Atmospheres*, 121, 457–477,
1363 <https://doi.org/10.1002/2015JD023711>, 2016.
- 1364 Zilker, B., Richter, A., Blechschmidt, A.-M., von der Gathen, P., Bougoudis, I., Seo, S., Bösch, T.,
1365 and Burrows, J. P.: Investigation of meteorological conditions and BrO during ozone
1366 depletion events in Ny-Ålesund between 2010 and 2021, *Atmospheric Chemistry and*
1367 *Physics*, 23, 9787–9814, <https://doi.org/10.5194/acp-23-9787-2023>, 2023.
- 1368
- 1369